Cooperative Dynamic Jahn-Teller Effect. I. Molecular Field Treatment of Spinels

R. Englman and B. Halperin
Soreq Nuclear Research Centre, Yavne, Israel
(Received 26 May 1969; revised manuscript received 7 August 1969)

A theory of cubic-to-tetragonal transformations occurring in spinels containing octahedrally coordinated (*B* site) d^9 and d^4 transition-metal ions in high concentration is developed. The problem is treated in the spirit of the molecular field approximation. For each Jahn-Teller (JT) susceptible ion in the unit cell, a Schrödinger equation is solved, in which the variables of the octahedra (the occupancies of the degenerate states or the distortion from cubic symmetry) appear as temperature-dependent unknown averages. These are then determined self-consistently, utilizing the solution of the Schrödinger equation. The present treatment introduces two improvements on the previous theories given by Wojtowicz and Kanamori. The first is to take into account the dynamic JT effect, thus covering a much wider experimental range, including moderate or even weak anisotropic (nonlinear) JT couplings. The other innovation is the inclusion of the excited vibronic states. Five characteristic regions of solution are distinguished; (a) the static limit, to which previously studied cases belong; (b) the three-state region, which differs from the previous one in that it allows the splitting between the lowest doublet and singlet to become comparable to the molecular field energy; (c) the general regime: the anisotropic energy, the kinetic energy, and the molecular field are of the same order of magnitude (all the excited vibronic states must be taken into account); (d) the strong molecular field limit; (e) the Ising-model limit of weak molecular field, in which case the ground vibronic doublet alone needs to be considered. Thermodynamic quantities such as the specific heat and entropy of transition, as well as bulk distortion at different temperatures and concentrations, are computed and compared with those obtained from previous theories. The phase transition is of first order, but in regimes (d) and (e) the transition entropy is very small. The first-order transition temperature reduces, as a result of introducing dynamic effects, to about half the value obtained by Wojtowicz. A digest of the experimental data is given in an Appendix.

I. INTRODUCTION

The spinel structure (Fig. 1) represents probably the most frequent example of oxides in which a low-temperature low-symmetry phase occurs because of the collective operation of the Jahn-Teller (JT) effect. The existence of a transition to this phase has been established in a considerable number of compounds and by a variety of techniques, including x-ray crystallography, neutron scattering, electrical conductivity, infrared spectroscopy, calorimetric measurements, and the quadrupole splitting in the Mössbauer spectra. A (possibly incomplete) list of compounds and references, as well as some additional information, can be found in Tables II–IV of this work. In the compounds covered by the list the low-temperature distortion is due to paramagnetic cations, notably Mn^{3+} and Cu^{2+}, in a doubly degenerate electronic state (*E*) situated at octahedrally coordinated sites of the spinel. It appears from perusal of the list and of the literature quoted that, while the very fact of macroscopic distortion associated with JT ions in finite concentration has been known for some time, more recent work has added details to our knowledge, especially through the employment of a greater variety of techniques and the more precise establishment of the distribution of competing cations at the various sites (e.g., through taking data after quenching the spinel). Still, wishing to be honest, we should admit that

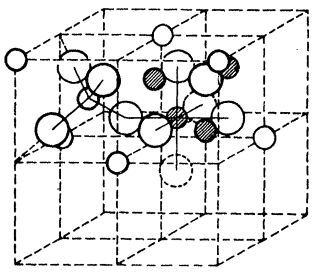

FIG. 1. Unit cell of a normal spinel AB_2O_4. Ions situated in two octants are shown, the ions drawn by broken circles belong to other octants. Large circles are oxygen ions; small shaded circles are metal ions *B* at octahedral sites; small open circles are metal ions *A* at tetrahedral sites. [From E. W. Gorter, Philips Res. Rept. 9, 295 (1954).]

the motivation for this investigation is not the dynamics of the experimental situation, but the statics of the theoretical front.

Following the recognition by Dunitz and Orgel[1] and by McClure[2] of the connection between the lowering of symmetry in transition-metal oxides and the JT effect, later elaborated by Goodenough in his book,[3] theories for the mechanism of the observed phase transition were put forward by Finch, Sinha, and Sinha,[4] by Wojtowicz,[5] and by Kanamori[6] in terms of an order parameter, which was in fact the occupancy of one of the degenerate states. In the first formulation[3] a two-fold degeneracy was assumed, while in the later improved versions, a threefold orientational degeneracy was considered for each paramagnetic center. It will be shown that in this conception of the problem the interaction between the centers leads to a highly anisotropic Heisenberg model. The molecular field approximation[7] was used by the preceding authors,[4-6] as well as in two more recent works,[8] to solve the cooperative problem. In this work we also use this approximation, leaving more efficient techniques to a forthcoming work. These techniques should incorporate short-range correlation, which is neglected in the molecular field approach, and which should thereby provide the key to the low-symmetry fields, observed,[9,10] e.g., in Mössbauer experiments. The origin of these fields is the local distortion which is present also in the disordered phase,[11] although in some magnetic crystals an alternative interpretation[12] is also possible due to magnetostriction.

If the molecular field approximation is unreliable as regards local effects, it should, nevertheless, be sufficient to explain such macroscopic effects as the change at the transition point of the crystallographical axial ratio c/a and its variation with temperature. However, even here we find some discrepancies, such as the existence of a minimal critical concentration of JT ions which is not predicted by the present theory. This subject is also postponed for later consideration.

In the present work we introduce two major changes compared to previous theories, and a few minor ones. First, we shall treat the cooperative distortion as arising from a dynamic, rather than a static, JT effect. In the relatively high-temperature region ($\geq 100\,^{\circ}\mathrm{K}$), with which we are mainly concerned here, the static JT effect is exceptional in molecular or quasimolecular complexes; in cooperative manifestations of the effect where a given amount of distortion is shared out among a great number of modes (of the lattice), this finding is likely to apply even more forcefully. This justifies, in our view, the reconsideration of the problem through a dynamic treatment.

The other essential innovation is the inclusion of the excited vibronic states. In the cited works[5,6] only the three lowest vibronic states were considered: These states coalesce in the static limit to three equivalent distortions, one along each of the cubic axes. In the higher-lying states the system tends to resonate between the distortions. Raising the temperature so as to populate these states will have a disordering effect. This effect is additional to that acting within the ground triplet, which achieves disorder through increase of the entropy. The inclusion of the excited states leads then to a reduction of the transition temperature.

The minor novelties which emerge enroute are the derivation of a Heisenberg-like coupling model appropriate to the static limit, the development of a microscopic quantitative model for the pairwise interaction[5] between adjacent octahedra in Sec. II, and the solution of the vibronic problem in a reduced tetragonal symmetry (D_4 in our case) in Sec. III.

The arrangement of the work is as follows: In Sec. II we explain the operation of the JT effect in a somewhat simplified model of the spinel structure and treat the cooperative problem in the static limit, which will be tackled from an angle different from those of Refs. 5 and 6. We next introduce the Schrödinger equation for the vibronic problem (Sec. III) first for a complex in undistorted octahedral, then in distorted tetragonal surroundings. The macroscopic aspects of the phase transitions are found in Sec. IV. In Sec. V we introduce the five categories in which the problem falls, that is, depending on the values of the parameters, and we present our results, many of these in graphical form, referring these categories to experimental information as far as possible. Unfortunately, the experimental data are insufficiently detailed to allow us to make quantitative comparisons, such as would produce, for example, significantly better agreement than that contained already in Ref. 5 or that would enable us to determine the parameters of the systems unambiguously. It is hoped, however, that the large variety of behavior which the dynamic effects introduce will prompt further experimental explorations.

II. EFFECTIVE COUPLING IN SPINELS

We refer to Fig. 1 in the Introduction to show the spinel structure. We now confine our attention to normal spinels. The framework of B-site ions is then situated on four fcc sublattices whose lattice points lie, respectively, on [000], [110], [101], and [011]. We suppose the B cations to be doubly

degenerate JT ions. The A cations, if in nondegenerate states, do not cause directly any distortions, and therefore we shall disregard them in the following. Through this procedure we reduce the unit cell to one-quarter of its original size: It now contains four B cations (labeled I–IV) and eight anions (labeled 1–8), as shown in the Fig. 2. Had we included the A-type ions, we would have found that their packing pressure affects different anions in the original unit cell by different amounts.

In Fig. 2(b) the oxygen octahedra round the B ions situated in a unit cell are completed by borrowing anions from the neighboring unit cells. If we recall that each of the I–IV cation types forms a fcc lattice and agree to label the unit-cell position by a vector, which is in fact, the radius vector of the position of one of the cations (e.g., I) then we realize that for the octahedra of the $\vec{n}$th cell, eight anions are borrowed from eight neighboring unit cells.

In Fig. 2(b) the labeling of the anions includes the unit cell to which they belong.

We assume for the purpose of the discussion of the static limit of the JT effect, [13] that the octahedra surrounding each B cation undergo a tetragonal distortion along an X, Y, or Z direction.

We shall next construct the Hamiltonian, including the elastic energy due to interactions between nearest neighbors and more distant ions and the vibronic coupling terms, but excluding the kinetic energy, since we shall first treat the static limit. By minimizing the energy we shall be able to eliminate the ionic coordinates and shall derive a Heisenberg-like Hamiltonian which exhibits the interaction between the occupancies of $|E_\theta\rangle$ or $|E_\epsilon\rangle$ states on neighboring cations. This Hamiltonian can then form the basis of the statistical mechanical problem, in the static limit, as in the work of Wojtowicz. [5]

The JT term expressing the linear coupling between the electronic states of the cation and the coordinates of the anions[13] is $\frac{1}{2}L(M\omega/\hbar)^{1/2}$ times

$$(12)^{-1/2}\,\sigma_\theta(\vec{n},\mathrm{I})\{2[Z(\vec{n},3) - Z(\vec{n}-a\hat{y}-a\hat{z},7)] - [X(\vec{n},5)-X(\vec{n},1)] - [Y(\vec{n},2)-Y(\vec{n}+a\hat{x}-a\hat{z},6)]\} + \tfrac{1}{2}\sigma_\epsilon(\vec{n},\mathrm{I})\{[X(\vec{n},5)-X(\vec{n},1)] - [Y(\vec{n},2)-Y(\vec{n}+a\hat{x}-a\hat{z},6)]\}$$

and analogous terms involving $\sigma_\theta(\vec{n},\mathrm{II})$, ..., $\sigma_\epsilon(\vec{n},\mathrm{IV})$.

The small Cartesian displacements of the ith anion ($i=1,\ldots,8$) in the $\vec{n}$th unit cell are denoted by $X(\vec{n},i)$, etc. $\sigma_\theta(\vec{n},j)$, $\sigma_\epsilon(\vec{n},j)$ ($j=\mathrm{I},\ldots,\mathrm{IV}$) are the Pauli matrices

$$\begin{pmatrix}-1 & 0\\ 0 & 1\end{pmatrix},\quad \begin{pmatrix}0 & 1\\ 1 & 0\end{pmatrix},$$

operating in the function space of the doubly degenerate one-electron orbitals E_θ, E_ϵ of the jth cation in the $\vec{n}$th cell. In the factor multiplying the previous expression M is the effective mass and ω is the frequency characterizing the cation-anion stretching. These quantities arise from the elastic term, which takes the form

$$\tfrac{1}{2}M\omega^2\{[X(\vec{n},5)-X(\vec{n},\mathrm{I})]^2+[Y(\vec{n}+a\hat{x}-a\hat{y},6) - Y(\vec{n},\mathrm{I})]^2+\text{similar terms}\},$$

(one term for each nearest-neighbor cation-anion bond). The coefficient L will be discussed later.

It is necessary to include, in addition to these central forces between nearest neighbors, also forces which are noncentral or which act between nonnearest neighbors. In the absence of these forces the distortions of different octahedra do

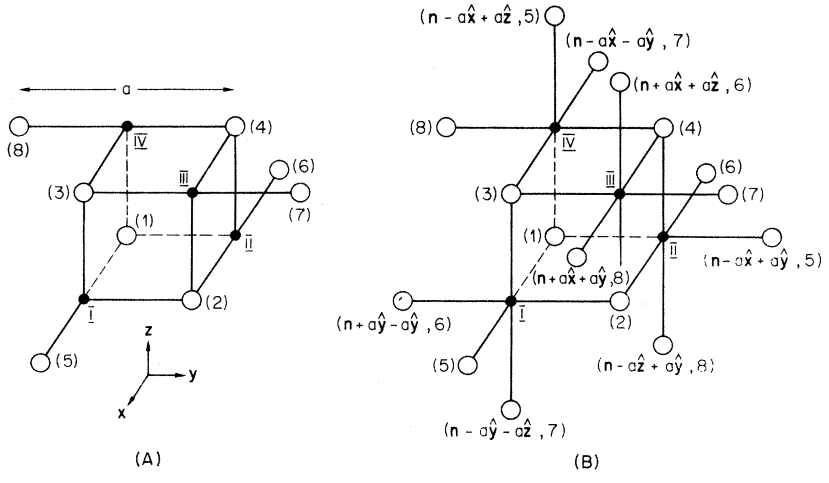

FIG. 2. Structure of the reduced unit cell in spinels without A cations; (a) showing the labeling of the ions in the reduced nth unit cell; (b) showing also the anion borrowed from the neighboring reduced unit cells so as to complete the octahedra.

not interfere with one another and cooperative phenomena are not possible. Analytically, the simplest farther neighbor force which will provide coupling between octahedra is a central force opposing the displacement of the (1) anion and acting in the direction of the III cation, i.e., along the body diagonal [see Fig. 2(a) for labeling], with analogous forces for the rest of the anions.[14] In symbols, this force contributes to the Hamiltonian terms of the type

$$H_{\rm int} = \tfrac{1}{2}\lambda M\omega^2[X(\vec{n},1)+Y(\vec{n},1)+Z(\vec{n},1) - X(\vec{n},\mathrm{III})-Y(\vec{n},\mathrm{III})-Z(\vec{n},\mathrm{III})]^2 , \qquad (1)$$

and similar terms for other body diagonals within the unit cell. λ is a number which compares the strength of this force to that of nearest-neighbor forces. It is a measure of cooperative forces.

We shall now extremize the potential energy with respect to nuclear displacements of the anions, assuming at the same time that the cations are fixed. This assumption may be viewed in one of the two ways. It can be regarded as an extreme formulation of the physical fact that the cationic geometry in spinels depends not only on the nearest-neighbor anionic configuration, but also on the positions of next-neighbor cations as well as those of farther ions. Alternatively, the following treatment of the phase transition may be viewed as exact, but subject to a microscopic constraint on each cation. The true physical situation is then that obtained by relaxing the constraint. However, in the ordered phase the constraint due to stretching forces is zero to the first order, since then anion 1 is displaced perpendicularly to the line connecting it to cation III. Also, in the disordered phase the average constraint is zero. Thus one can hopefully expect that the imposition of an artificial constraint will only have a modest quantitative significance, similar in amount perhaps to the neglect of anharmonic coupling between different modes.

The extremization yields expressions for anionic displacements in terms of the Pauli matrices of the three neighboring cations. When these expressions are substituted back into the Hamiltonian, one obtains the following coupling terms {as multiples of $[\lambda/(1+3\lambda)]L^2/4\hbar\omega$}:

Coupling between I–II: $\frac{1}{6}\sigma_\theta(\mathrm{I})\sigma_\theta(\mathrm{II}) - \frac{1}{2}\sigma_\epsilon(\mathrm{I})\sigma_\epsilon(\mathrm{II})$;

Coupling between III–IV: $\frac{1}{6}\sigma_\theta(\mathrm{III})\sigma_\theta(\mathrm{IV}) - \frac{1}{2}\sigma_\epsilon(\mathrm{III})\sigma_\epsilon(\mathrm{IV})$;

Coupling between I–III: $-\frac{1}{3}\sigma_\theta(\mathrm{I})\sigma_\theta(\mathrm{III}) - (1/\sqrt{12})[\sigma_\epsilon(\mathrm{I})\sigma_\theta(\mathrm{III})+\sigma_\epsilon(\mathrm{III})\sigma_\theta(\mathrm{I})]$;

Coupling between I–IV: $-\frac{1}{3}\sigma_\theta(\mathrm{I})\sigma_\theta(\mathrm{IV}) + (1/\sqrt{12})[\sigma_\epsilon(\mathrm{I})\sigma_\theta(\mathrm{IV})+\sigma_\epsilon(\mathrm{IV})\sigma_\theta(\mathrm{I})]$; (2)

Coupling between II–III: $-\frac{1}{3}\sigma_\theta(\mathrm{II})\sigma_\theta(\mathrm{III}) + (1/\sqrt{12})[\sigma_\epsilon(\mathrm{II})\sigma_\theta(\mathrm{III})+\sigma_\epsilon(\mathrm{III})\sigma_\theta(\mathrm{II})]$;

Coupling between II–IV: $-\frac{1}{3}\sigma_\theta(\mathrm{II})\sigma_\theta(\mathrm{IV}) - (1/\sqrt{12})[\sigma_\epsilon(\mathrm{II})\sigma_\theta(\mathrm{IV})+\sigma_\epsilon(\mathrm{IV})\sigma_\theta(\mathrm{II})]$.

The symbol $\vec{n}$ denoting the unit cell has been omitted at this juncture from the designation of the Pauli matrices $\sigma_i(\vec{n},\mathrm{I})$, since the same coupling exists between any pair of similarly oriented nearest-neighbor cations whether or not they are in the same unit cell.

It is interesting to find that the coupling terms between I and II are simply proportional to

$$\sigma_{\theta x}(\mathrm{I})\sigma_{\theta y}(\mathrm{II})+\sigma_{\theta y}(\mathrm{I})\sigma_{\theta x}(\mathrm{II}) .$$

Here $\sigma_{\theta x}$ and $\sigma_{\theta y}$ are the transformed σ_θ matrices with the x and y axes chosen as axis of quantization. Coupling expressions between other pairs of ions can be got by appropriate transformations from the I–II coupling.

To interpret the coupling we note, following Wojtowicz,[5] that there are four possible types of interactions between a pair of octahedra which have two corners in common. These interactions may be described by reference to the previous figure, Fig. 2(b), as follows. Let the octahedron about the I cation be elongated along the Z axis. Then we find the following interaction energies between this octahedron and another one elongated as shown in Table I.

In Ref. 5 the following interaction energy relations were conjectured $V_{12} < V_{11} < V_{22} < V_{21}$, whereas we have derived from our model $V_{12} < V_{21} < V_{11} < V_{22}$.

Note added in manuscript. In a recent work [P. Novak, J. Phys. Chem. Solids 30, 2357 (1969)] two more sets of inequalities between V_{ij} were postulated, different from either inequality written out above. However, Novak's work is not based on a quantitative model and it was taken for granted in it that, in our expression [Eq. (2)] for

TABLE I. Pair interaction energies.

Octahedron	Long axis	Interaction energy in units of $\lambda L^2/4(1+3\lambda)\hbar\omega$	Wojtowicz's symbol
III	Z	$-\frac{1}{3}$	V_{12}
III	X	$-\frac{1}{12}$	V_{21}
II	Z	$\frac{1}{6}$	V_{11}
IV	X	$\frac{5}{12}$	V_{22}

coupling between I and II, both terms are necessarily negative.

It is possible to regard the coupling terms in Eq. (2) as an anisotropic Heisenberg-Hamiltonian coupling the "spins" on various cations. The usual treatments of statistical mechanics can then be accorded to this Hamiltonian, e.g., as was done by Wojtowicz, through the adaptation of the molecular field method. This amounts to deriving a pair of self-consistent equations for the averages $\bar{\sigma}_\theta$, $\bar{\sigma}_\epsilon$ of the Pauli matrices of one of the cations, say of $(\vec{n}, \mathrm{I})$:

$$\bar{\sigma}_\theta = \frac{-\exp[-A\bar{\sigma}_\theta] + \frac{1}{2}\exp[-A(-\frac{1}{2}\bar{\sigma}_\theta + \frac{1}{2}\sqrt{3}\bar{\sigma}_\epsilon)] + \frac{1}{2}\exp[-A(-\frac{1}{2}\bar{\sigma}_\theta - \frac{1}{2}\sqrt{3}\bar{\sigma}_\epsilon)]}{\exp[-A\bar{\sigma}_\theta] + \exp[-A(-\frac{1}{2}\bar{\sigma}_\theta + \frac{1}{2}\sqrt{3}\bar{\sigma}_\epsilon)] + \exp[-A(-\frac{1}{2}\bar{\sigma}_\theta - \frac{1}{2}\sqrt{3}\bar{\sigma}_\epsilon)]} ,$$

$$\bar{\sigma}_\epsilon = \frac{-\frac{1}{2}\sqrt{3}\exp[-A(-\frac{1}{2}\bar{\sigma}_\theta + \frac{1}{2}\sqrt{3}\bar{\sigma}_\epsilon)] + \frac{1}{2}\sqrt{3}\exp[-A(-\frac{1}{2}\bar{\sigma}_\theta - \frac{1}{2}\sqrt{3}\bar{\sigma}_\epsilon)]}{\exp[-A\bar{\sigma}_\theta] + \exp[-A(-\frac{1}{2}\bar{\sigma}_\theta + \frac{1}{2}\sqrt{3}\bar{\sigma}_\epsilon)] + \exp[-A(-\frac{1}{2}\bar{\sigma}_\theta - \frac{1}{2}\sqrt{3}\bar{\sigma}_\epsilon)]} ,$$

where $A \equiv [\lambda/(1+3\lambda)]L^2/4\hbar\omega kT$.

In these equations, the expressions for the coupling energies [Eq. (2)] have been utilized, in which, however, the matrices of all cations, except of $(\vec{n}, \mathrm{I})$, have been replaced by the average values $\bar{\sigma}_\theta$, $\bar{\sigma}_\epsilon$.

The equations represent thermal averages of σ_θ, σ_ϵ in three possible electronic states of $(\vec{n}, \mathrm{I})$ associated with the three distortions of its octahedron. When extending our treatment to include dynamic effects (as in Sec. III and thereafter) one of our main endeavors was to generalize in an appropriate way the above self-consistent equations. As will appear in Eq. (9), the proper long-range order parameters to replace $\bar{\sigma}_\theta$, $\bar{\sigma}_\epsilon$ are the mean distortional coordinates. Discussion of the solution of Eq. (3) will be given later (in the end of Sec. III) as limiting cases of the more general treatment.

III. INCLUSION OF DYNAMIC EFFECTS

In the dynamic (or vibronic) approach to the JT effect the kinetic energy is included and the ionic displacements are regarded as quantum-mechanical dynamic variables. A major simplification in the kinetic-energy expression results if we now also make the assumption, introduced and briefly discussed in Sec. II, that the cations are held rigidly. Further, we can refer each cation-anion *stretching* uniquely to one octahedral complex (we ignore at the present the transverse force constants due to their being small compared to the radial ones), and we can pass on to the next step, which will pave the way for the molecular field approximation.

We lift out of the total Hamiltonian of the crystal the term $H(\vec{n}, \mathrm{I})$ which contains the normal coordinates of the cation I in the $\vec{n}$ unit cell. $H(\vec{n}, \mathrm{I})$ consists of three parts: The first part contains those stretching motions, with respect to a cation, which do not enter the JT effect (e.g., an odd vibrational motion or a perfectly symmetric one, with reference to a single cation). This part will be irrelevant to the treatment which follows and we shall not consider it. Then there is a part $H_0(\vec{n}, \mathrm{I})$, including the kinetic, elastic, and JT coupling, which arises from the stretching motion of the anions (with respect to a single cation) that gets coupled to the electronic state of the cation. This part is identical to the Hamiltonian of an isolated octahedral complex and will indeed be written in a notation appropriate to the normal modes of such a complex.

Finally, we have the farther neighbor term H_{int}, Eq. (1), which couples different JT distortions around different cations. We have found there that such a term is necessary to cause any cooperative effect at all. Here we shall rewrite it in the normal coordinates of each octahedron around its cation.

For the second part considered earlier we write

$$\begin{aligned} H_0(\vec{n}, \mathrm{I}) = {} & \tfrac{1}{2}\hbar\omega \\ & \times\left(-\frac{\partial^2}{\partial q_\theta^2(\vec{n}, \mathrm{I})} - \frac{\partial^2}{\partial q_\epsilon^2(\vec{n}, \mathrm{I})} + q_\theta^2(\vec{n}, \mathrm{I}) + q_\epsilon^2(\vec{n}, \mathrm{I})\right) \\ & + \tfrac{1}{2}L[q_\theta(\vec{n}, \mathrm{I})\sigma_\theta(\vec{n}, \mathrm{I}) + q_\epsilon(\vec{n}, \mathrm{I})\sigma_\epsilon(\vec{n}, \mathrm{I})] \\ & + \tfrac{1}{4}K\{[q_\epsilon^2(\vec{n}, \mathrm{I}) - q_\theta^2(\vec{n}, \mathrm{I})]\sigma_\theta(\vec{n}, \mathrm{I}) \\ & + 2q_\theta(\vec{n}, \mathrm{I})q_\epsilon(\vec{n}, \mathrm{I})\sigma_\epsilon(\vec{n}, \mathrm{I})\} \\ & + \tfrac{1}{4}\sqrt{2}\,N[3q_\theta(\vec{n}, \mathrm{I})q_\epsilon^2(\vec{n}, \mathrm{I}) - q_\theta^3(\vec{n}, \mathrm{I})] . \end{aligned} \tag{4}$$

Hamiltonians of this type have been extensively discussed in original papers on the JT effect[15-23] or in the reviews.[24-26] Here ω is the frequency of the vibrational modes whose coordinates $q_\theta(\vec{n}, \mathrm{I})$, $q_\epsilon(\vec{n}, \mathrm{I})$ (or q_θ, q_ϵ for short) have been written in reduced dimensionless form in units of the zero-point motion amplitude $(\hbar/M\omega)^{1/2}$, where M is the effective mass of the vibration. The coefficients L (for linear), K (for quadratic), and N

(for cubic) have all the same dimension (energy) and are given in terms of the derivatives of the electronic potential V by

$$L=-\left\langle E_\theta\left|\frac{\partial V}{\partial q_\theta}\right|E_\theta\right\rangle+\left\langle E_\epsilon\left|\frac{\partial V}{\partial q_\theta}\right|E_\epsilon\right\rangle ,$$
$$K=\left\langle E_\theta\left|\frac{\partial^2 V}{\partial q_\theta^2}\right|E_\theta\right\rangle-\left\langle E_\epsilon\left|\frac{\partial^2 V}{\partial q_\theta^2}\right|E_\epsilon\right\rangle ,$$
$$N=-\tfrac{1}{6}\sqrt{2}\left(\left\langle E_\theta\left|\frac{\partial^3 V}{\partial q_\theta^3}\right|E_\theta\right\rangle+\left\langle E_\epsilon\left|\frac{\partial^3 V}{\partial q_\theta^3}\right|E_\epsilon\right\rangle\right)$$

Here $|E_\theta\rangle$ and $|E_\epsilon\rangle$ are the *one-electron* doublet kets which transform as $(2z^2-x^2-y^2)/\sqrt{6}$ and $(x^2-y^2)/\sqrt{2}$, respectively.

The introduction of a new set of coefficients calls for some comment in view of the proliferation of existing symbols. When the invariant coupling terms in the Hamiltonian Eq. (4) are built up in a standard manner by the use of the V coefficients,[27] then the coefficients of the invariants in Eq. (4) are given uniquely. They are as shown above. The method of constructing the invariants will be published elsewhere.[26,26]

The point-group classification will be according to the molecular symmetry group O. Actually, as we shall be dealing with octahedrally coordinated B-site cations in spinels, we ought to add g or u subscripts appropriate to the (approximate) O_h symmetry. However, we shall forgo this encumbrance for the sake of simplicity,

We note that in the static limit,[13] which is attained by letting the mass $M\to\infty$ and by neglecting the kinetic energy, the equilibrium condition is given by $q=q_0\equiv L/2\hbar\omega$, and the stabilization energy by $E_{JT}=L^2/8\hbar\omega$. Under conditions of strong linear coupling $L/\hbar\omega\gg 1$ the Hamiltonian of Eq. (4) can be approximately diagonalized by transforming to a new set

$$|\psi_-\rangle=\cos\tfrac{1}{2}\varphi|E_\theta\rangle-\sin\tfrac{1}{2}\varphi|E_\epsilon\rangle ,$$
$$|\psi_+\rangle=\sin\tfrac{1}{2}\varphi|E_\theta\rangle+\cos\tfrac{1}{2}\varphi|E_\epsilon\rangle .$$

Here φ is the angle in the polar form of the vibrational coordinates

$$q_\theta=q\cos\varphi \quad\text{and}\quad q_\epsilon=q\sin\varphi .$$

Whether $|\psi_-\rangle$ or $|\psi_+\rangle$ appears in the low-lying states depends on the sign of the linear coupling coefficient. It is usually accepted that the coefficient L of the one-electron matrix is positive, $L>0$. Then the low-lying vibronic states take the form

$$\Psi=q^{-1/2}\chi_{n_q}(q-q_0)\chi(\varphi)|\psi_-\rangle ,$$

where χ_{nq} is the n_q'th oscillator wave function [energy $E_q=(n_q+\frac{1}{2})\hbar\omega-L^2/8\hbar\omega$] representing oscillation across the potential trough which lies on a circle of radius q_0. The $\chi(\varphi)$ is the angular factor whose Schrödinger equation reads in the strong linear coupling limit

$$q_0=L/2\hbar\omega\gg 1,\quad |q-q_0|/q_0\ll 1 ,$$
$$\left(-\alpha\frac{\partial^2}{\partial\varphi^2}-\beta\cos 3\varphi+E_q\right)\chi(\varphi)=E\chi(\varphi) . \tag{5}$$

Here $\alpha=\hbar\omega/2q_0^2$

and
$$\beta=-(\tfrac{1}{4}Kq_0^2-\tfrac{1}{4}\sqrt{2}\,Nq_0^3)$$
$$=-[L^2/16(\hbar\omega)^3](\hbar\omega K-\tfrac{1}{2}\sqrt{2}\,NL) . \tag{6}$$

In the limit of strong nonlinear coupling, where $\beta/\alpha\gg 1$, the system performs small oscillations about the minima of the potential $-\beta\cos 3\varphi$. For Mn^{3+} in the configuration d^4, calculations analogous to those by Öpik and Pryce[13] for $Cu^{2+}(d^9)$ indicate that $\beta>0$. Then the minima are at $\varphi=0$, $\pm\frac{2}{3}\pi$.

We return now to the term $H_{\rm int}$ of Eq. (1) describing the interference between JT distortions on different octahedra. We let the cationic coordinates $X(\vec{n}, \mathrm{III})$, etc., take the value 0:

$$H_{\rm int}=\tfrac{1}{2}\lambda\hbar\omega\left[\left(-\tfrac{1}{2}q_\epsilon(\vec{n},\mathrm{I})+\frac{1}{2\sqrt{3}}q_\theta(\vec{n},\mathrm{I})\right.\right.$$
$$\left.+\tfrac{1}{2}q_\epsilon(\vec{n},\mathrm{II})+\frac{1}{2\sqrt{3}}q_\theta(\vec{n},\mathrm{II})-\frac{1}{\sqrt{3}}q_\theta(\vec{n},\mathrm{IV})\right)^2$$
$$\left.+\text{five similar terms}\right] . \tag{7}$$

As indicated in Sec. II, the method of the molecular field theory is applied by replacing all normal coordinates in $H(\vec{n}, \mathrm{I})$ other than $q_\theta(\vec{n}, \mathrm{I})$ and $q_\epsilon(\vec{n}, \mathrm{I})$ by the averages $\bar{q}_\theta$ and $\bar{q}_\epsilon$. This step leads to

$$H_{\rm int}=\tfrac{1}{2}\lambda\hbar\omega[q_\theta^2(\vec{n},\mathrm{I})+q_\epsilon^2(\vec{n},\mathrm{I})-2q_\theta(\vec{n},\mathrm{I})\bar{q}_\theta$$
$$-2q_\epsilon(\vec{n},\mathrm{I})\bar{q}_\epsilon+\bar{q}_\theta^2+\bar{q}_\epsilon^2] . \tag{8}$$

The averages are defined by

$$\bar{q}_\iota=\mathrm{Tr}[q_\iota(\vec{n},\mathrm{I})e^{-H(\vec{n},\mathrm{I})/kT}]/\mathrm{Tr}e^{-H(\vec{n},\mathrm{I})/kT} ,$$
$$\iota=\theta,\epsilon . \tag{9}$$

These definitions introduce a self-consistency in the formalism. However, the Hamiltonian is now dependent on the temperature T through the presence of the averages $\bar{q}_\iota$ in it. The state of the system at any temperature is given by the solution of the Schrödinger equation whose Hamiltonian is $H(\vec{n}, \mathrm{I})$ but which now also contains the averages defined above. We shall see that above a certain temperature, which we shall denote by T_t, the averages $\bar{q}_\theta$ and $\bar{q}_\epsilon$ vanish, corresponding to the nondistorted configuration representing the thermodynamically stable state of the system. Below T_t, nonzero values of $\bar{q}_\iota$ represent the stable states.

Before presenting the thermodynamics of the situation we point out a practical simplification which can be made so as to let the equations be

manageable. The cubic symmetry of the problem may be utilized to put $\bar{q}_\epsilon = 0$ in the Schrödinger equation. The solutions with $\bar{q}_\theta \neq 0$ then describe states with z-oriented tetragonal distortions. Solutions with $\bar{q}_\epsilon \neq 0$ are completely equivalent to these, except that they describe x- and y-oriented distortions and they are much harder to come by since not only the Hamiltonian is more involved, but there are now two self-consistency equations, Eq. (9), to solve.

The Schrödinger equation for the vibrational factor $\chi(\varphi)$, which is written in Eq. (5) for O symmetry, takes the following form for the z-oriented solutions:

$$\left(-\alpha\frac{\partial^2}{\partial\varphi^2} - \beta\cos 3\varphi - \gamma_\theta\cos\varphi + E_q + \frac{\gamma_\theta^2}{2\lambda\hbar\omega q_0^2}\right)\chi(\varphi) = E\chi(\varphi) \,. \tag{10}$$

The definition of α was given following Eq. (5), β is shown in Eq. (6), and we have already noted that for Mn^{3+} at octahedral sites $\beta > 0$. The γ_θ is related to the thermal average of $\cos\varphi (\equiv q_\theta/q_0)$ by the relation

$$\gamma_\theta \equiv \lambda\hbar\omega q_0 \bar{q}_\theta = \langle\cos\varphi\rangle \lambda\hbar\omega q_0^2 \,. \tag{11}$$

The eigenvalue equation, Eq. (10), was solved by numerical matrix diagonalization using the set of orthogonal states

$$\cos\tfrac{1}{2}(2m-1)\varphi, \quad \sin\tfrac{1}{2}(2m-1)\varphi$$
$$m = 1, 2, \ldots \,.$$

The eigenenergies are shown in Figs. 3(a), 3(b), and 3(c) as function of the tetragonal field strengths and for three values $\beta/\alpha = 0.4$, 4.0, and 20.0.

Interpreting the curves, e.g., positive γ_θ, and referring to the drawings which follow (Fig. 4), we can say that the upward or downward slope of each curve in Fig. 3 at any value of the abscissa gives an estimate of the relative percentage for the system being, for that state and that γ_θ/α, in the wells at $\varphi = 0$ and at $\varphi = \pm\frac{2}{3}\pi$. Consider, for example, the level indicated in Fig. 4.; for zero or low tetragonal field strengths this level has negligible slope. This conforms to the situation in Fig. 4 (a) where the state is approximately equally shared by the three wells. As the tetragonal field strength grows to the situation shown in Fig. 4(b), and the asymmetry of the potential wells becomes perceptible, the indicated level will become localized in *either* of the two wells, acquiring thereby a non-negligible slope. Subsequently, as in Fig. 4(c) the level sinks down into the well at $\varphi = 0$ and the curve bends over to a steady downward slope. In this last region the downward-sloping levels are uniformly spaced harmonic oscillator levels of the $\varphi = 0$ well.

Some progress is possible in analytical terms in the three-state approximation, i.e., if one retains only the three lowest vibronic states. For nonlinear and strong linear coupling the following matrix has been obtained[18,25] for these states:

$$\begin{array}{c} |\Psi_\theta\rangle \\ |\Psi_\epsilon\rangle \\ |\Psi_{A_1}\rangle \end{array}\begin{bmatrix} -q\gamma_\theta & 0 & r\gamma_\theta \\ 0 & q\gamma_\theta & 0 \\ r\gamma_\theta & 0 & 3\Gamma \end{bmatrix} \,. \tag{12}$$

Here q and r are the reduction factors introduced by Ham.[25] (See also Refs. 29–35.) His definitions refer to the lowest-lying vibronic doublet $(\Psi_\theta, \Psi_\epsilon)$ and the singlet Ψ_{A_1} immediately above them

$$q = -\left\langle\Psi_\theta\middle|\begin{pmatrix}-1 & 0\\ 0 & 1\end{pmatrix}\middle|\Psi_\theta\right\rangle \,,$$
$$r = \left\langle\Psi_{A_1}\middle|\begin{pmatrix}-1 & 0\\ 0 & 1\end{pmatrix}\middle|\Psi_\theta\right\rangle \,.$$

3Γ is the energy difference between the lowest vibronic doublet and the next singlet in the three-state approximation. For extremely strong linear coupling q and r can be redefined in terms of the vibrational factor χ as follows:

$$q = \langle\chi_\theta|\cos\varphi|\chi_\theta\rangle \,, \quad r = -\langle\chi_{A_1}|\cos\varphi|\chi_\theta\rangle \,.$$

In what we have just called "the three-state approximation," one finds that

$$q = \tfrac{1}{2}e^{-1/(8\nu)}(1+2\gamma)/(1+\gamma) \,,$$
$$r = (-1/\sqrt{2})e^{-1/(8\nu)}(1-\gamma)/[(1+\gamma)(1-2\gamma)]^{1/2} \,,$$

where $\nu \equiv (9\beta/8\alpha)^{1/2}$ and $\gamma = e^{-2\nu\pi^2/9}$.

Computed values of q and r obtained from numerical solution of the Schrödinger equation, Eq. (5), are shown in Figs. 5 and 6. These are compared with the analytical expressions shown above which, we recall, are based on the three-state approximation.

In the same approximation, the vibronic eigenenergies of Eq. (5) are found to be

$$\frac{E_E}{\alpha} = \frac{E_q}{\alpha} + \nu - \frac{4\nu^2\pi^2}{9}\frac{\gamma}{1+\gamma} + \frac{8\nu^2}{9}e^{-9/8\nu}\frac{1-\gamma}{1+\gamma}$$

for the doublet, and for the next singlet

$$\frac{E_{A_1}}{\alpha} = \frac{E_q}{\alpha} + \nu + \frac{8\nu^2\pi^2}{9}\frac{\gamma}{1-2\gamma} + \frac{8\nu^2}{9}e^{-9/8\nu}\frac{1+2\gamma}{1-2\gamma} \,.$$

The energy difference 3Γ between these is

$$3\Gamma \equiv E_{A_1} - E_E = 3\beta\gamma[\pi^2\tfrac{1}{2}(1+\gamma) - 2e^{-9/8\nu}] \,.$$

This expression is dominated by the first positive term showing that the doublet is lower.

The energy eigenvalues and expectation values of $\cos\varphi$ from matrix (12) are

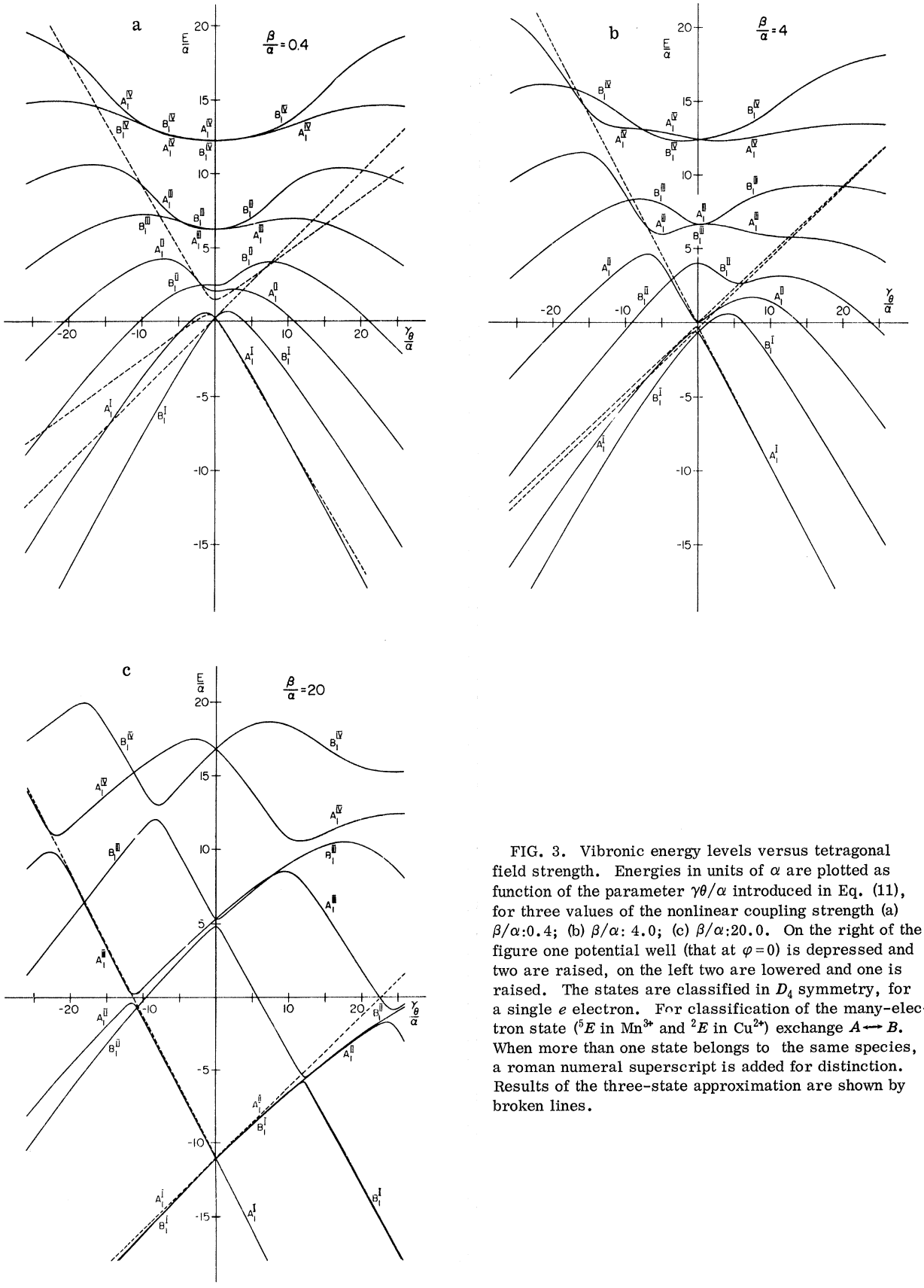

FIG. 3. Vibronic energy levels versus tetragonal field strength. Energies in units of α are plotted as function of the parameter $\gamma\theta/\alpha$ introduced in Eq. (11), for three values of the nonlinear coupling strength (a) β/α:0.4; (b) β/α: 4.0; (c) β/α:20.0. On the right of the figure one potential well (that at $\varphi=0$) is depressed and two are raised, on the left two are lowered and one is raised. The states are classified in D_4 symmetry, for a single e electron. For classification of the many-electron state (^5E in Mn^{3+} and ^2E in Cu^{2+}) exchange $A \rightleftharpoons B$. When more than one state belongs to the same species, a roman numeral superscript is added for distinction. Results of the three-state approximation are shown by broken lines.

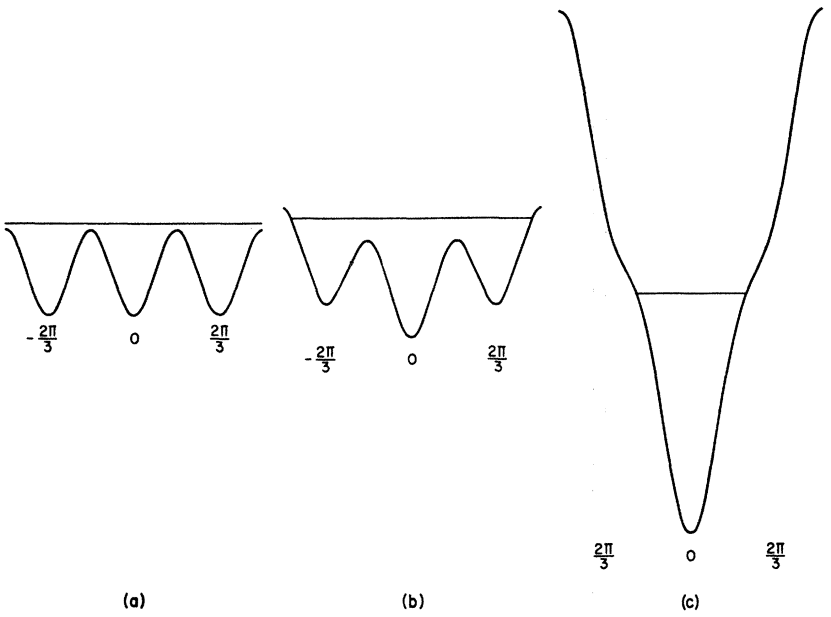

FIG. 4. Behavior of a moderately high-lying state as the tetragonal field strength increases. Figure shows a section of the potential on the circle $q = q_0$.

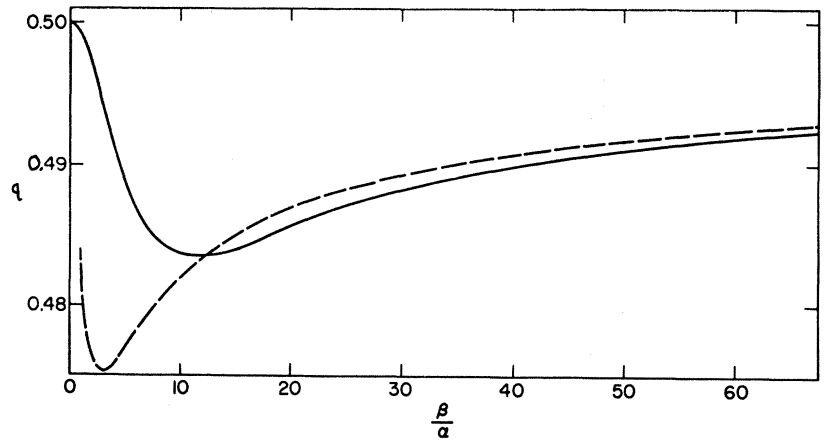

FIG. 5. q versus β/α. Diagonal reduction factor q is defined in the text. Exact computed values are shown by full lines and the results of the three-state approximation by broken lines down to $\beta/\alpha = 1$ at which value the approximation is not expected to be valid any longer.

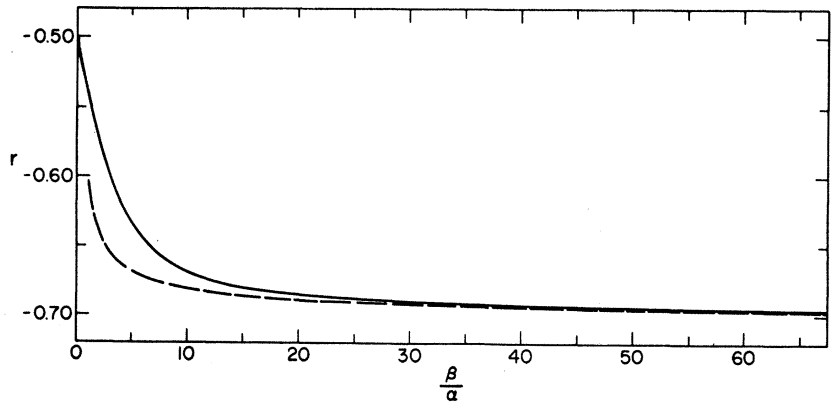

FIG. 6. r versus β/α. The r is the off-diagonal reduction factor defined in the text. The exact values, and those obtained in the three-state approximation of r, are shown.

$$E_1 = E_E + \gamma_\theta q \quad ,$$

$$\begin{pmatrix} E_2 \\ E_3 \end{pmatrix} = E_E + \tfrac{1}{2}(3\Gamma - \gamma_\theta q) \pm \tfrac{1}{2}[\gamma_\theta^2(q^2+4r^2) + 2(3\Gamma)\gamma_\theta q + (3\Gamma)^2]^{1/2} \quad ,$$

$$\langle \Psi_1 | \cos\varphi | \Psi_1 \rangle = -q \quad ,$$

$$\begin{pmatrix} \langle \Psi_2 | \cos\varphi | \Psi_2 \rangle \\ \langle \Psi_3 | \cos\varphi | \Psi_3 \rangle \end{pmatrix} = \tfrac{1}{2}q \mp \frac{(3\Gamma)q + \gamma_\theta(q^2+4r^2)}{2[\gamma_\theta^2(q^2+4r^2) + 2(3\Gamma)\gamma_\theta q + (3\Gamma)^2]^{1/2}} \quad .$$

Here E_E is the energy of the ground-state doublet.

While the explicit analytical formulation of Eq. (9) in the three-state limit can have its uses, e.g., for demonstrating the first-order nature of the transition (for this see Sec. IV), we prefer not to encumber these pages by long expressions. Rather, we quote the results for the extremely strong nonlinear coupling limit, which was also treated in Refs. 5 and 6, namely, when $3\Gamma \to 0$. Then Eq. (9), for $\iota = \theta$ and $\bar{q}_\epsilon = 0$, becomes

$$v = (e^u - e^{-u/2})/(e^u + 2e^{-u/2}) \tag{13}$$

with the abbreviations

$$u = \gamma_\theta/kT \quad \text{and} \quad v = \gamma_\theta/\lambda\hbar\omega q_0^2 \, .$$

It will be seen by referring to Eq. (3) in the static treatment that it is the same as Eq. (13) (if $\bar{\sigma}_\theta = -v$ and $\bar{\sigma}_\epsilon = 0$), except that the coupling parameter there differs from the present one by a factor $(1+3\lambda)^{-1}$. This arises because in the dynamic treatment, $H_{\rm int}$ was treated perturbationally, correct to λ, while in Sec. II this was done correct to all orders in λ. Since very likely $\lambda \ll 1$, there is no essential disagreement.

Equation (13) yields the axial distortion and pressure, both of which are proportional to γ_θ, when the tetragonal axis is z. Two equivalent sets of equations, with $\bar{q}_\epsilon \neq 0$ and $\gamma_\epsilon \neq 0$, could be written for tetragonal distortions along x or y.

As the discussion of Sec. IV shows, the transition temperature T_t is determined from $F(\gamma_{\theta,t}) = F(0)$. (At T_t all temperature-dependent parameters will bear the subscript t.) It can be shown that this equation, whose two sides are the definite integrals of the two sides of Eq. (9) from 0 to $\gamma_{\theta,t}$, becomes $\frac{1}{2}u_t v_t = \ln\frac{1}{3}(e^{u_t} + e^{-u_t/2})$. The simultaneous solution of this with Eq. (13) yields

$$u_t = \tfrac{4}{3}\ln 2, \quad v_t = \tfrac{1}{2} \, .$$

The quantity

$$kT_t/\lambda\hbar\omega q_0^2 = v_t/u_t = 3/8\ln 2 = 0.54$$

is the "reduced transition temperature" featuring in Wojtowicz's paper.[5] (See also the same quantity called "normalized transition temperature" in Fig. 9.)

IV. THERMODYNAMICS

The phase transition is best discussed by starting with the Helmholtz free-energy function F defined for the assembly of octahedra by

$$e^{-F/kT} = \mathrm{Tr} e^{-H(\vec{n},\mathrm{I})/kT} \, .$$

As defined earlier in Eq. (4), $H(\vec{n}, \mathrm{I})$ is the Hamiltonian for the octahedron for the I cation in the $\vec{n}$ unit cell (see Fig. 2); the Hamiltonian of any other octahedron would, of course, be similar. This construction of $H(\vec{n}, \mathrm{I})$ was achieved in Sec. III at the cost of considering the cations fixed and of disregarding the normal modes not relevant to the JT effect. The interference due to neighboring octahedra appears in $H(\vec{n}, \mathrm{I})$ through the presence of the *individual* normal displacements of the neighbors as in Eq. (7), or of the *mean* normal displacements, $\bar{q}_\theta$ and $\bar{q}_\epsilon$, as in Eq. (8). As regards each octahedron this displacement is felt by it as a constraint externally imposed on it. No other constraint is applied on the shapes of the octahedra (there is, though, the condition fixing the cations), so the thermodynamical variables conjugate to $\bar{q}_\theta$ and $\bar{q}_\epsilon$ are zero, or

$$\frac{\partial F}{\partial \bar{q}_\theta} = 0, \quad \frac{\partial F}{\partial \bar{q}_\epsilon} = 0 \, . \tag{14}$$

These are also the equations defining thermal equilibrium. However, it can be seen from the form of the Hamiltonian, Eqs. (4) and (8), that these two equations are in fact identical to the Eq. (9) defining $\bar{q}_\theta$ and $\bar{q}_\epsilon$, our so-called self-consistency equations. This is very gratifying.

It will be shown presently that the transition from the cubic to the low-temperature tetragonal phase is of the first order as required by the Landau theory of phase transitions.[36,37] The transition occurs at that temperature T_t at which the free energies of the cubic phase (when $\bar{q}_\theta = \bar{q}_\epsilon = 0$) and of the tetragonal phase ($\bar{q}_\theta \neq 0$) become equal:

$$F(\bar{q}_\theta = 0) = F(\bar{q}_\theta \neq 0) \, . \tag{15}$$

This equation is additional to Eq. (9), the self-consistency conditions which hold at any temperature. The connection between the equations may be understood by reference to Fig. 7. Here the S-shaped curves are the right-hand side of Eq. (9) plotted as function of the tetragonal field parameter γ_θ for three temperatures. Intersections of these curves with the left-hand side of Eq. (9) occur at nonzero values of γ_θ as well as $\gamma_\theta = 0$. The former values represent the stable thermodynamic state only at a temperature $T = T_t$ such that the two areas bounded by the two curves

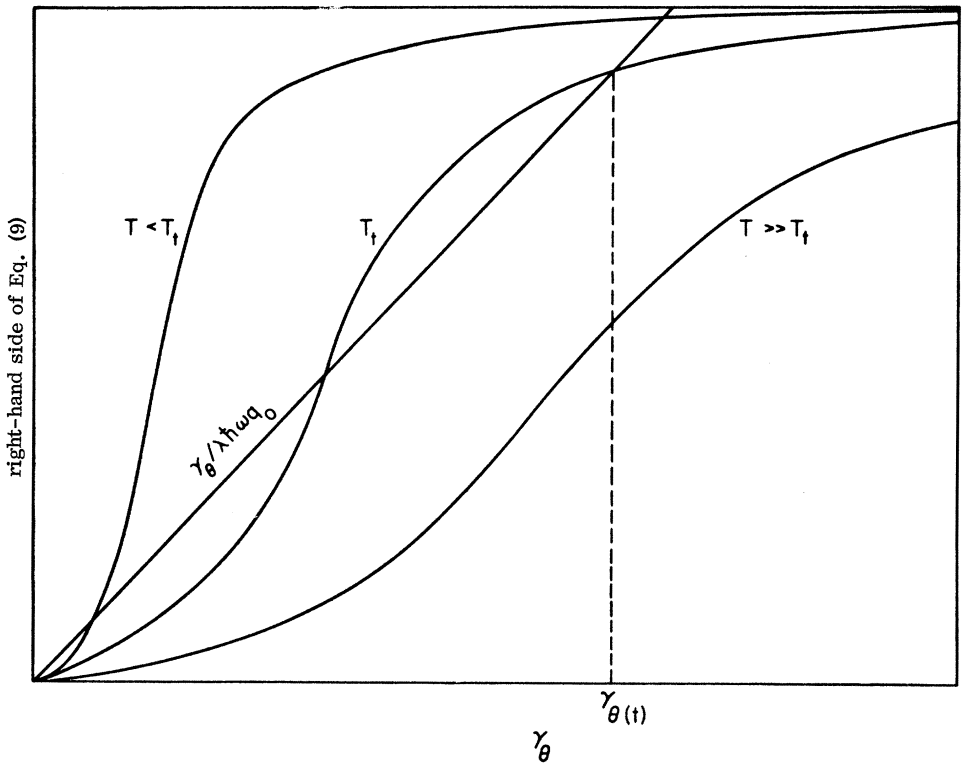

FIG. 7. Graphical solution of Eq. (9) (for explanation see text).

become equal to each other, here $F(\bar{q}_\theta) = F(0)$, or at temperatures below this. For $T > T_t$, $\gamma_\theta \neq 0$ can at best represent a metastable state.

In order that an S-shaped curve be obtained, it is necessary that in the expansion of the right-hand side of Eq. (9) near $\gamma_\theta = 0$, the coefficient of the quadratic term in γ_θ should be positive.

Making use of the analytical expressions for the eigenvalues and expectation values obtained earlier in the three-state approximation, we have for the right-hand side of Eq. (9) up to second order in γ_θ

$$\frac{1}{2+\exp(-3\Gamma/kT)}\left[\gamma_\theta\left(\frac{1-\exp(-3\Gamma/kT)}{(3\Gamma)}\right)2r^2 + \gamma_\theta^2\left(\frac{\exp(-3\Gamma/kT)+3\Gamma/kT-1}{(3\Gamma)^2}\right)3qr^2\right].$$

The expression in the last large parentheses is necessarily positive; the above discussion shows the transition to be of the first order.

Each of the equal areas referred to above is a measure of the heat of transition. In our results this turns out to be small, when compared with the energy of alignment of the distortion in the direction of the molecular field. [This energy is of the order of the area of a triangle which has a dotted line for one of its sides (Fig. 7).]

It is of interest to digress in order to see graphically (Fig. 8) the shape of the low-symmetry phase when the cations are assumed to be held fixed to their position in the cubic phase. A planar cross section at $X = 0$ of Fig. 2 is shown. It is apparent that the effect of the constraint is to bend the Mn-O-Mn angles to less than a right angle. If the bending force constants are zero (as has been assumed provisionally above), then this situation is innocent; however, in reality, the angles will become right angles as shown in the figure on the right [Fig. 8(b)]. Under the latter condition, we have $c/a > 1$ in the crystal.

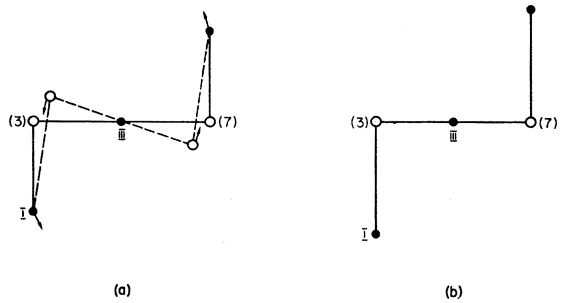

FIG. 8. Distorted arrangement of anions when the cations are fixed. Positions of the ions in a plane section containing the ions I, 3, III, 7, etc., are shown (refer to Fig. 2 for the meaning of labeling) (a) when the cations are in the cubic positions; (b) after the relaxation of the cations.

Returning now to the thermodynamics of the phase transition, we note that the specific heat C, defined by $C = T(\partial S/\partial T)$, where S is the entropy, will behave discontinuously across the transition. It will possess a δ function about $T = T_t$ of such magnitude as to provide a finite heat of transition, given by $T_t \Delta S$, where ΔS is the entropy change.

It should be remarked that the specific heat is at constant volume since the distortion leaves the volume of the octahedra constant. More importantly, the specific heat is under conditions of a constraint so imposed as to keep the cations at the positions occupied by them in the cubic phase. When this constraint is relieved, the specific heat changes by an amount given by

$$C(\sigma_3 = 0) - C\left(\epsilon_3 = \frac{2(a-c)}{c+2a}\right) = T\left(\frac{\partial \epsilon_3}{\partial T}\right)^2 \frac{\partial^2 W}{\partial \epsilon_3^2} \ .$$

The specific heats on the left-hand side are, respectively, in the relaxed tetragonal state of the lattice, when the applied axial stress σ_3 is zero, and in the state in the ordered phase, which is so obtained as to be macroscopically cubic. This latter state is achieved by letting the strains take the values

$$\epsilon_3 = -2\epsilon_1 = -2\epsilon_2 = 2(a-c)/(c+2a) \ .$$

The Voigt notation is used for the strains ϵ_i and stress σ_i.[38] On the right, W is the elastic energy.

The above relation is analogous to and is similarly derivable as the well-known result for $C_p - C_v$.[39] In terms of the Lamé elastic constant μ, which refers to the same volume as the specific heats,

$$C_{\sigma_3} - C_{\epsilon_3} = 4T\mu\left(\partial \frac{(a-c)/(c+2a)}{\partial T}\right)^2 .$$

V. RESULTS AND DISCUSSION

Before presenting the results of the calculations, we should describe in general terms the different ranges of physical parameters (corresponding to diverse physical situations) which lead to different types of solutions and may even require different methods for solution. Assuming strong linear coupling $L/\hbar\omega \gg 1$, we are left essentially with three independent energy parameters: α, the rotational energy [see Eq. (5)]; β, the nonlinear coupling energy, being a measure of the depth of the angular minima in the q_θ, q_ϵ plane [see Eq. (6)]; $\lambda\hbar\omega q_0^2$, the molecular field strength or, more accurately, its temperature-independent factor [see Eq. (11)]. However, the physical situation is not necessarily best described by these parameters, but rather by combinations of them. Thus for strong linear coupling we have the computed energy ΔE, the separation between the lowest cubic singlet and doublet. This reduces in the three-state limit to

$$3\Gamma \equiv 3\beta\gamma\left[\tfrac{1}{2}\pi^2(1+\gamma) - 2\exp(-9/8\nu)\right]$$

(for ν and γ see Sec. III).

For strong nonlinear coupling we have the parameter $3(2\alpha\beta)^{1/2}$, the separation between the sets of threefold nearly degenerate levels of Eq. (5). In terms of the preceding parameters we mark out the following regimes:

(*a*) *Static limit.* This is characterized by $\beta \gg \alpha$ and $\Delta E \sim 3\Gamma \ll \lambda\hbar\omega q_0^2 \ll 3(2\alpha\beta)^{1/2}$. To this region belongs Wojtowicz's treatment of the cooperative problem, in which α was taken as zero, leading to a completely degenerate vibronic triplet ($3\Gamma = 0$). For comparison between his molecular field parameter zV and ours, we can write $\frac{2}{9}zV = \lambda\hbar\omega q_0^2$. In this regime this is the only significant energy parameter, and $kT_t/\lambda\hbar\omega q_0^2 = 0.54$.[5]

(*b*) *Three-state region.*

$$\beta \gtrsim \alpha, \quad \Delta E \sim 3\Gamma \sim \lambda\hbar\omega q_0^2 \ll 3(2\alpha\beta)^{1/2} \ .$$

Here the kinetic energy α may become comparable to β, so the treatment must be dynamic throughout, the splitting between the lowest doublet and singlet may be of a similar order of magnitude to that of the molecular field, but the latter is still much smaller than the spacing between the threefold nearly degenerate levels. This last fact allows us to remain in the three lowest vibronic levels, neglecting the contribution from the excited vibronic states.

Another physically important energy parameter enters in this region, the tunneling energy 3Γ. This lowers the transition temperature.

(*c*) *General regime.* The molecular field energy $\lambda\hbar\omega q_0^2$ is sufficiently large to cause excitation into several high-lying states. This comprises $\beta \gg \alpha$, provided $\lambda\hbar\omega q_0^2 \gtrsim 3(2\alpha\beta)^{1/2}$, and $\beta \lesssim \alpha$, provided $\lambda\hbar\omega q_0^2 \gtrsim \Delta E$ (including cases where α, β, and $\lambda\hbar\omega q_0^2$ are of similar magnitude). kT_t is now no longer linear with $\lambda\hbar\omega q_0^2$.

(*d*) *Strong molecular field limit.* It is possible to treat this limit analytically as in the Appendix. The molecular field energy is the only significant energy here and $kT_t/\lambda\hbar\omega q_0^2 = 0.5$, which is numerically similar to A, yet physically very different.

(*e*) *Ising-model limit.* $\Delta E \sim \alpha \gtrsim \beta$ and $\lambda\hbar\omega q_0^2 \ll \alpha$. The lowest doublet E is alone populated. Here the transition heat tends to zero and the transition to second-order type. $kT_t/\lambda\hbar\omega q_0^2 \to q^2$, where q is the reduction factor ($q \lesssim \frac{1}{2}$) defined in Sec. III. The q represents in this limit an additional parameter of the system.

Rigorously speaking, the transition is of the first order in all five regimes (*a*)–(*e*) in accordance with the Landau theory.[36,37] However, under

TABLE II. Spinel data for $Mn^{3+}(d^4, {}^5E$ ground state) at B sites (ΔH is the latent heat of transition in kcal/mole, ΔS is the entropy change in cal/mole deg).

Compound	Probable formula	Methods of measurement	T_t (°K)	c/a at Room Temperature	c/a near T_t	Thermal data	Critical concentration at Room Temperature
Mn_3O_4	$Mn^{2+}[Mn_2^{3+}]O_4$	X ray [a–d] Electrical conductivity [b] Thermal measurements [a,b,e] Infrared spectroscopy [f]	1443	1.15–1.16	1.13 [c]	$\Delta H = 4.5–5$ [a,e] $\Delta S = 5.1–3.5$ [a,e]	
$Mn_3O_4–MgAl_2O_4$ [g]	Varying $Mg_z^{2+}Mn_{1-z}^{2+}[Mn_2^{3+}]O_4$, $(0 \le z < 1)$ [h]	X ray		1.11–1.16			0.58
$Mg_zMn_{3-z}O_4$	$Mg^{2+}[Mn_2^{3+}]O_4$, $(z=1,\ T<1070$ [a])	X ray [a,h–j]		1.15–1.16		$\Delta H = 3.5$ [a]	
	$Mg_{0.55}^{2+}Mn_{0.45}^{3+}[Mg_{0.45}^{2+}Mn_{1.55}^{3+}]O_4$ $(z=1,\ T=T_t$ [a]) $Mg_{0.51}^{2+}Mn_{0.49}^{3+}[Mg_{0.49}^{2+}Mn_{1.51}^{3+}]O_4$ ($z=1$, when quenched from 1520 °K [i])	Electrical conductivity [h] Thermal measurements [a]	1123–1443	1.147 ($z=1$ [j])	≤ 1.16 [a]	$\Delta S = 3.1$ [a]	
$MgMn_2O_4–MgAl_2O_4$ [k]	Varying	X ray		1.10–1.15			0.59
$MgGa_{2-z}Mn_zO_4$ [l]	Varying	X ray and neutron scattering	>1123	~1.02	~1.15		~0.5
$MgCr_{2-z}Mn_zO_4$ [l]	Varying	X ray and neutron scattering	>1123	~1.02	~1.15		0.48
$Zn_zMn_{3-z}O_4$	$Zn_z^{2+}Mn_{1-z}^{2+}[Mn_2^{3+}]O_4$ [a,h], $(0 \le z \le 1)$	X ray [a,f,h] Electrical conductivity [h]	1120–1470 [h]	1.11–1.16	1.15 [a] ($z=1$)	$\Delta H = 5$ [a] ($z=1$)	
	$Zn^{2+}[Zn_{z-1}^{2+}Mn_{2-z}^{4+}Mn_{4-2z}^{3+}]O_4$ [h] $(1 \le z < 1.2)$	Thermal measurements [a] Infrared spectroscopy [f]	1323 ($z=1$ [a])			$\Delta S = 3.8$ [a] ($z=1$)	
$Zn_zGe_{1-z}Mn_2O_4$ [d]	$Zn_{0.6}^{2+}Ge_{0.4}^{4+}[Mn_{0.8}^{2+}Mn_{1.2}^{3+}]O_4$ ($z=0.6$)	X ray Magnetic data		1.15			0.6
$Zn_zGe_{1-z}Co_{2-2z}Mn_{2z}O_4$ $(0 \le z \le 1$ [d])	$Zn_z^{2+}Ge_{1-z}^{4+}[Co_{2-2z}^{2+}Mn_{2z}^{3+}]O_4$	X ray Magnetic data	700–1300	≤ 1.144			0.65
$Fe_{3-z}Mn_zO_4$	$Mn_z^{2+}Fe_{1-z}^{3+}[Mn_{z-t}^{3+}Fe_{1-t}^{2+}Fe_{1-z+2t}^{3+}]O_4$ [m,n] $Mn_{0.8}^{2+}Fe_{0.2}^{2+}[Fe_{1.8}^{3+}Mn_{0.2}^{3+}]O_4$ ($z=1$ [o])	X ray [o,p] Mössbauer effect [n]	≥670	1.15	1.06–1.13		~0.60 [c]
$Co_{3-z}Mn_zO_4$	$Co^{2+}[Co_{2-z}^{3+}Mn_z^{3+}]O_4$ $(0 \le z < 2$ [d])	X ray [a,b,d] Electrical conductivity [a]	600–1443 [b]			$\Delta H = 3.5$ ($z=2$ [a])	
	$Co_{3-z}^{2+}Mn_{z-2}^{2+}[Mn_2^{3+}]O_4$ $(2 \le z \le 3$ [d])	Thermal measurements [d] Magnetic data [a,b]	1173 ($z=2$ [a])	1.03–1.16 [b]		$\Delta S = 3.0$ ($z=2$ [a])	0.56 [b]
$Cu_zCo_{1-z}Mn_2O_4$ [j]	$Co_{1-z}^{2+}Cu_z^{2+}[Mn_2^{3+}]O_4$	X ray	1173 ($z=0$)	1.123 ($z=0$)			$z=0.53$
$Cu_zCd_{1-z}Mn_2O_4$ [j]	$Cd_{1-z}^{2+}Cu_z^{2+}[Mn_2^{3+}]O_4$	X ray		1.200 ($z=0$)			$z=0.48$
$Cu_zMg_{1-z}Mn_2O_4$ [j]	$Mg_{1-z}^{2+}Cu_z^{2+}[Mn_2^{3+}]O_4$	X ray	1123 ($z=0$)	1.147 ($z=0$)			$z=0.28$
$Cu_zZn_{1-z}Mn_2O_4$ [j]	$Zn_{1-z}^{2+}Cu_z^{2+}[Mn_2^{3+}]O_4$	X ray	1323 ($z=0$)	1.142 ($z=0$)			$z=0.85$

[a] Reference 40.
[b] Reference 42.
[c] Reference 45.
[d] Reference 46.
[e] J. C. Southard and G. E. Moore, J. Am. Chem. Soc. 64, 1769 (1942).
[f] K. Siratori and Y. Aiyama, J. Phys. Soc. Japan 20, 1962 (1965).
[g] Reference 17.
[h] Reference 41.
[i] R. Manaila and P. Pausescu, Phys. Status Solidi 9, 385 (1967).
[j] S. T. Kshirsagar and A. B. Biswas, J. Phys. Chem. Solids 28, 1493 (1967).
[k] Reference 47.
[l] M. Grenot and M. Huber, J. Phys. Chem. Solids 28, 2441 (1967).
[m] Reference 4.
[n] M. Tanaka, T. Mizoguchi, and Y. Aiyama, J. Phys. Soc. Japan 18, 1091 (1963).
[o] L. Cervinka, S. Krupicka, and V. Synecek, J. Phys. Chem. Solids 20, 167 (1961).

TABLE III. Spinel data for Cu^{2+} (d^9, ^2E ground state) at B sites (ΔH and ΔS as in Table II).

Compound	Probable formula	Methods of measurement	T_t(°K)	c/a at Room Temperature	c/a near T_t	Thermal data	Critical concentration
$CuFe_2O_4$	$Fe^{3+}[Cu^{2+}Fe^{3+}]O_4$ [a]	X ray [a–d]	663 [e]		1.01 [c]		
		Thermal measurements [e]	After quenching:	1.03–1.06 [a–c]		$\Delta H = 0.25$ [e]	0.38 [b]
	$Fe^{3+}_{1-t}Cu^{2+}_t[Cu^{2+}_{1-t}Fe^{3+}_{1+t}]O_4$ [b]	Mössbauer effect [c]	363, [c] 633 [b]		1.03 [b]		
		Neutron scattering [a]					
$CuFe_{2-z}Cr_zO_4$		X ray [b,d]					
$z < 1$	$Fe^{3+}_{1-t}Cu^{2+}_t[Cu^{2+}_{1-t}Fe^{3+}_{1+t-z}Cr^{3+}_z]O_4$ [d]	Magnetic data [d]	220–630 [b,f]	1.04–1.06 [f]	1.02–1.04 [f]		0.38 [b]
		X ray					
$Ge_{0.2}Cu_{1.2}Fe_{1.6}O_4$ [g]		Mössbauer effect	783	1.075	1.05		

[a] E. Prince and R. G. Treuting, Acta Cryst. 9, 1025 (1956).
[b] Reference 44.
[c] T. Yamadaya, T. Mitui, T. Okada, N. Shikazono, and Y. Hamaguchi, J. Phys. Soc. Japan 17, 1897 (1962).
[d] S. Miyahara and H. Ohnishi, J. Phys. Soc. Japan 12, 1296 (1956).
[e] Reference 43.
[f] H. Ohnishi and T. Teranishi, J. Phys. Soc. Japan 16, 35 (1961).
[g] M. Tanaka, T. Mizoguchi, and Y. Aiyama, J. Phys. Soc. Japan 18, 1089 (1963).

conditions of β small compared either to α [which case may belong to (*c*)] or to the molecular field [as in (*d*)] the latent heat will be very small and the transition will appear experimentally as of the second order. Additionally, for β not small but $\lambda\hbar\omega q_0^2$ small enough, a similar situation may obtain, as already remarked under (*e*). Empirically, in all systems studied so far (see Tables II–IV) the latent heat was found sizable. The case $\beta = 0$ is that instance of the Landau theory when there is no third-order invariant in γ_θ, in which case a second-order transition is possible.

From the experimental transition temperatures (see Tables II–IV) one estimates $\lambda\hbar\omega q_0^2 \approx 1000\ \mathrm{cm}^{-1}$. Taking as typical values $\beta \approx 500\ \mathrm{cm}^{-1}$, $\alpha \approx 10\ \mathrm{cm}^{-1}$ [13] leads then to $\lambda\hbar\omega q_0^2/3(2\alpha\beta)^{1/2} \simeq 3$; this casts doubt on the applicability of our three-state approximation as well as on Wojtowicz's treatment. [5] The considered experimental systems belong to our general regime (*c*), with $kT_t/\lambda\hbar\omega q_0^2 \simeq 0.5$.

The graphical results are of three types. First the computed transition temperature is plotted against the *parameters* of the physical situation (Figs. 9 and 10). Then the *temperature dependence* of the specific heat (Fig. 11) and of the axial distortion (Fig. 12) is shown. Lastly, the behavior of the axial distortion as function of the *B-site concentration* of the JT ions is displayed.

Figure 9 exhibits the behavior of the normalized transition temperature (this is T_t divided by the molecular field strength $\lambda\hbar\omega q_0^2$) as function of the ratio of the molecular field to $(\alpha\beta)^{1/2}$ (the meaning of which has already been discussed). The curves are plotted for constant values of β/α and are the results of many energy-levels calculations.

In the extreme right of the figure, one can identify the strong molecular field limit [case (*d*)], which is characterized by $kT_t/\lambda\hbar\omega q_0^2 = \frac{1}{2}$, as deduced analytically in the Appendix.

As the ratio $\lambda\hbar\omega q_0^2/(\alpha\beta)^{1/2}$ decreases, a wide region of values for the normalized transition temperature is reached, from somewhat above 0.5, down to about 0.25, covering what we have called the general regime [case (*c*)].

A further decrease of this ratio allows one to restrict the considerations to the lowest two ground states only, as long as $\beta \lesssim \alpha$, coming to what we have called "the Ising-model limit" [case (*e*)], in which the normalized transition temperature approaches the values of 0.25, for very small values of β/α.

More generally the expectation values of $\cos\varphi$ in the degenerate ground-state components are $\pm q$, yielding a limiting self-consistent equation of the form: $\gamma_\theta/\lambda\hbar\omega q_0^2 = q\,\mathrm{tgh}(\gamma_\theta q/kT)$. This equation yields a second-order phase transition at a

TABLE IV. Spinel data for Cu^{2+} and Mn^{3+} at B sites (ΔH and ΔS as in Table II.)

Compound	Probable formula	Methods of measurement	T_t(°K)	c/a at room temperature	Critical composition at room temperature
	$Mn^{2+}[Cu_z^{2+}Mn_z^{4+}Mn_{2-2z}^{3+}]O_4$	X ray (Refs. 41 and 57)			
$Cu_zMn_{3-z}O_4$	$(0 \le z \le 0.2)$	Electrical conductivity (Ref. 41)	1320–1443	1.161	$z=0.58$
	$Mn_{1-z}^{2+}Cu_z^{2+}[Mn_2^{3+}]O_4$ (Ref. 57)	Thermal measurements (Ref. 57)			
$(ZnMn_2O_4)_{1-z}(Cu_2GeO_4)_z$ $(0 \le z \le 0.6)$ (Ref. 51)	$Zn_{1-z}Cu_z[Cu_zGe_zMn_{2-2z}]O_4$	X ray Neutron scattering	>300	1.07–1.15	$z=0.4$
$(Zn\ Mn_2O_4)_{1-z}(Zn\ CuGe\ O_4)_z$ $(0 \le z \le 0.6)$		X ray Neutron scattering	>300	1.04–1.15	$z=0.55$

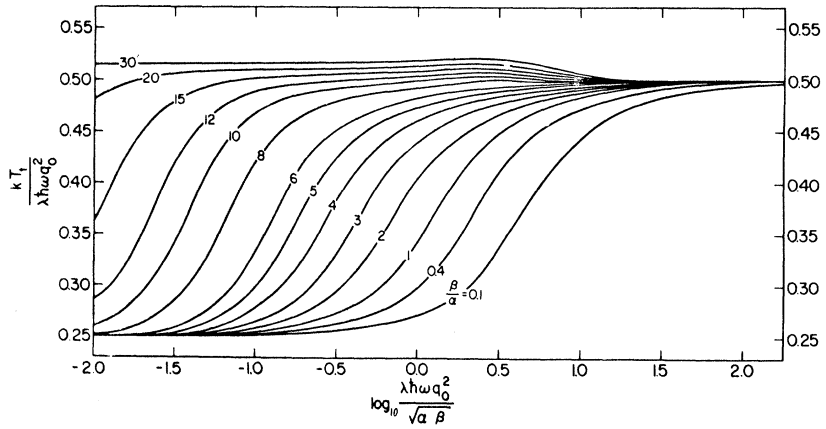

FIG. 9. Variation of the normalized transition temperature with the molecular field strength, plotted for different values of the nonlinear coupling.

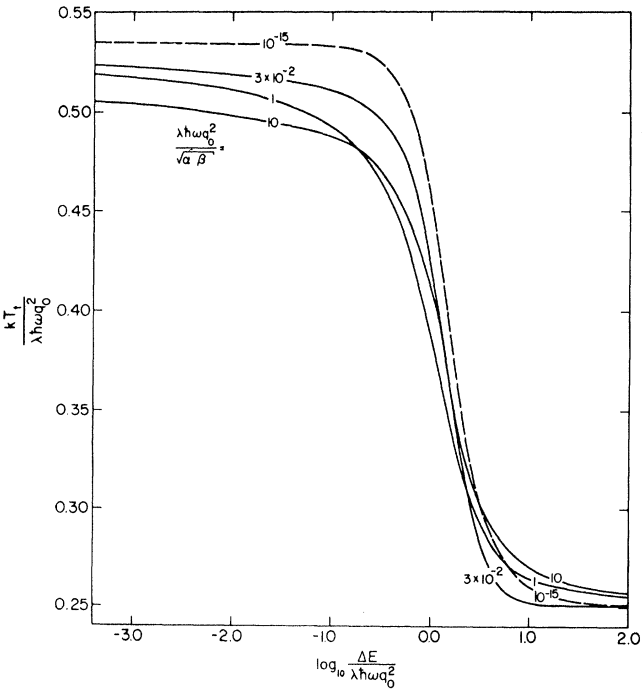

FIG. 10. Variation of the normalized transition temperature with the splitting between the doublet and singlet. Full curves show exact results; the broken curve is based on the three-state approximation, each curve for a fixed value of the parameter $\lambda\hbar\omega q_0^2/(\alpha\beta)^{1/2}$.

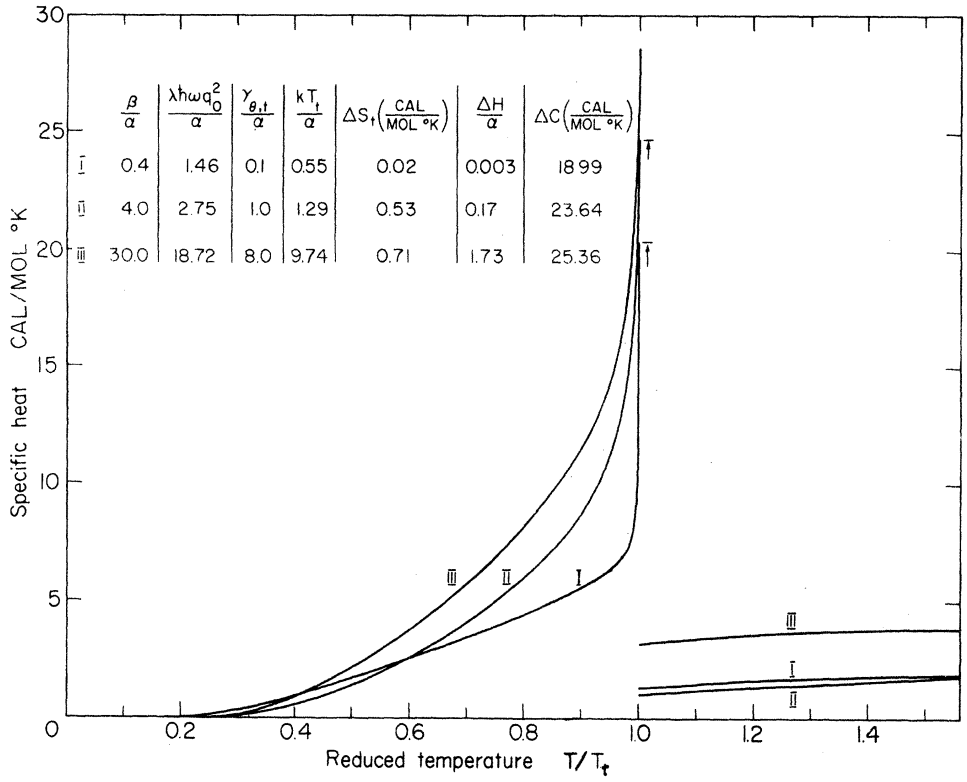

	$\frac{\beta}{\alpha}$	$\frac{\lambda\hbar\omega q_0^2}{\alpha}$	$\frac{\gamma_{\theta,t}}{\alpha}$	$\frac{kT_t}{\alpha}$	$\Delta S_t\left(\frac{\text{CAL}}{\text{MOL °K}}\right)$	$\frac{\Delta H}{\alpha}$	$\Delta C\left(\frac{\text{CAL}}{\text{MOL °K}}\right)$
I	0.4	1.46	0.1	0.55	0.02	0.003	18.99
II	4.0	2.75	1.0	1.29	0.53	0.17	23.64
III	30.0	18.72	8.0	9.74	0.71	1.73	25.36

FIG. 11. Specific heat versus reduced temperature for values of the physical parameters shown in the first two columns in the inset. Last five columns contain results obtained from the solution of Eqs. (9) and (15).

temperature defined by

$$kT_t/\lambda\hbar\omega q_0^2 = q^2, \quad (0.484 < q < \tfrac{1}{2})$$

When the concentrations of the JT ions at B-sites is less than unity ($0 < x < 1$), the molecular field strength defined for full concentration, i.e., for the spinel AB_2O_4, by $\lambda\hbar\omega q_0^2$ gets multiplied by x. Agreeing to a redefinition of λ which is proportional to x, we see in Fig. 9 how the transition temperature T_t changes with concentration. Regions in which T_t depends on x linearly, superlinearly, and sublinearly are noticed. (Note that $T_t/\lambda\hbar\omega q_0^2$ is plotted.) Experimentally a linear relation was observed in the mixed system of Co_3O_4-Mn_3O_4 (Ref. 40, Fig. 11), in $Cu_{2-2x}Mn_{1+2x}O_4$ (Ref. 41, Sec. III), and in the mixed oxides of the composition $Mg_zMn_{3-z}O_4$ (Ref. 41, Sec. 3.3). The concentration parameter z, $0 \leq z \leq 1$, is not identical with x defined in the previous paragraph, and specifies, partly, also the tetrahedral A-site ion concentration. The change in T_t here (or in $Zn_zMn_{3-z}O_4$) is rather slower than in the previous cases. On the other hand, a sublinear relation was observed in $Zn_{2-x}Mn_{1+x}O_4$ (Ref. 41, Sec. 3.2). A superlinear $T_t - x$ curve and the inadequacy of the theory of Ref. 5 to explain this were noted by Aoki[42] for the mixed Co and Mn spinels.

In order to clearly display the influence of the dynamic effect on the normalized transition temperature, we have plotted the latter in Fig. 10 against the ratio of ΔE (the energy splitting between lowest doublet and singlet) to the molecular field $\lambda\hbar\omega q_0^2$ for constant $\lambda\hbar\omega q_0^2/(\alpha\beta)^{1/2}$.

The figure includes results of calculations with many levels as well as three-level calculations (denoted by broken lines).

When $\Delta E (\simeq 3\Gamma)$ becomes negligible, one obtains the static limit [case (a)], in which the nor-

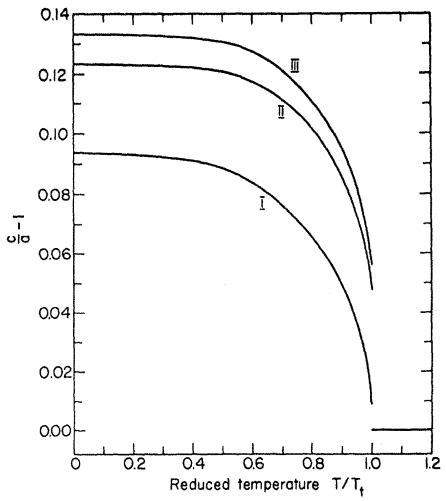

FIG. 12. Axial ratio as function of the reduced temperature. Parameters of the curves I, II, and III are as in Fig. 11.

malized transition temperature approaches 0.54, as was first obtained by Wojtowicz[5] and has already been discussed earlier in this work (see end of Sec. III). One can see from the figure that the smaller the ratio $\lambda\hbar\omega q_0^2/(\alpha\beta)^{1/2}$, the faster the static limit is approached.

An increase in the energy splitting $\Delta E \sim 3\Gamma$ brings us to the three-state region [case (*b*)], for which somewhat lower values than 0.54 for the normalized T_t are obtained.

As dynamic effects get enhanced, $\Delta E/\lambda\hbar\omega q_0^2$ increases further and the normalized transition temperature diminishes, ultimately to q^2, a value which characterizes the Ising-model limit [case (*e*)].

Figure 11 shows the temperature dependence of the specific heat for three different systems, denoted by I, II, and III, which are characterized by a small, medium, and high value of the nonlinear coupling β/α, respectively.

The datum in the inset gives also for each system the values of the following: $\lambda\hbar\omega q_0^2$ (the molecular field coupling coefficient), the transition parameter $\gamma_{\theta,t}$, the temperature kT_t, and ΔH (latent heat), all in units of α (the rotational energy), as well as the entropy change ΔS_t and the specific-heat discontinuity ΔC in cal/mole °K.

As was already stated, the λ-type curves possess a δ function about the transition point in order to provide a finite latent heat. This δ function is not shown in the figure.

Attention is directed to the rather abrupt λ shape of the specific-heat curve for small β/α (system I). It is as though for small β/α, most of the order-to-disorder transition (which is accompanied by negligible latent heat, thus experimentally simulating a second-order transition) occurs just in the vicinity of T_t.

For temperatures above T_t, the specific heat of systems with high β/α (system III) will reach the value of $1k$ (per site), as one expects for a one-dimensional harmonic oscillator. Further increase of the temperature will result in the population of higher-lying energy states, much above the potential barrier, thus enhancing the contributions from free-particle states and finally leading to a value of $\frac{1}{2}k$ for the specific heat. For small values of β/α, the shallow potential wells cause the specific heat to become somewhat above that of a free particle, as long as the temperature is not too high. At higher temperatures the limit of $\frac{1}{2}k$ per site will be reached here, too. We recall that in Ref. 5 where the system constantly resides at the bottom of the potential well, the specific heat is zero.

The specific-heat–at–constant-pressure curve and a heat of transition of 0.25 kcal/mole measured for $CuFe_2O_4$[43] are not in conflict with the theoretical values shown on Fig. 11; however, there is not sufficient information to determine the parameters of $CuFe_2O_4$ by comparing the experiment with our theory.

In order to obtain the temperature dependence of the lattice parameters we shall assume, following Wojtowicz,[5] that the c and the a parameters of the tetragonal average unit cell are, respectively, proportional to the mean lengths of the distorted octahedron's axes along and perpendicular to the z direction. Let l_0 be the length of the (undistorted) octahedral axis; then the above assumption means that

$$c \propto l_0 + Z_3 - Z_6, \quad a \propto l_0 + X_1 - X_4 = l_0 + Y_2 - Y_5 .$$

Replacing the anionic displacements X_i, Y_i, and Z_i by the normal coordinates Q_θ and Q_ϵ, averaging over different sites and putting $\overline{Q}_\epsilon = 0$, one obtains for the axial distortion

$$c/a - 1 = \sqrt{3}\ \overline{Q}_\theta/(l_0 - \overline{Q}_\theta/\sqrt{3}) .$$

We recall the relation $\overline{q}_\theta = (M\omega/\hbar)^{1/2}\overline{Q}_\theta$.

Figure 12 shows the axial ratio $c/a - 1$ as a function of the reduced temperature for the same three systems as before.

The ratio q_0/l_0 was taken to be 0.075 in our calculations which is thought to be a reasonable estimate for Mn^{3+} in spinels. The "saturation value" of $(c/a) - 1$ at absolute zero, which can be read off from the ordinate, differs quite considerably from one system to another, depending on the ground-state expectation values of $\cos\varphi$. In fact, the tetragonal distortion at 0 °K is completely determined by the integral q defined earlier in Sec. III; now, however, the state Ψ_θ is an eigenstate of a Hamiltonian containing also a tetragonal field. The strength of this field, as well as the value of β/α differ in the systems I, II, and III. When the value of $<\cos\varphi>$ approaches unity, we obtain a maximum value at 0 °K of 0.136 for $c/a - 1$, which is the maximum attainable value of the axial distortion in our model [in which $(q_0/l_0) = 0.075$].

The experimental curves of Ohnishi, Teranishi, and Miyahara[44] for $CuFe_{1.7}Cr_{0.3}O_4$, $CuFe_{1.8}Cr_{0.2}O_4$, and $CuFe_2O_4$ are similar to those in Fig. 12. In contrast, the $(c/a - 1)$ curves for mixed cobalt and copper oxides[42] and for Mn_3O_4, $MgMn_2O_4$, $ZnMn_2O_4$, and $CoMn_2O_4$[40] are essentially flat for most of the region $T < T_t$ and exhibit a drop to zero, only a few tens of degrees before T_t. The possibility that this behavior is due to short-range correlations will be investigated in a future work.

In Fig. 13 the effect of reduction of the JT-ion concentration x on the axial distortion is displayed for constant temperature. Curves are related to system III (whose parameters are given in

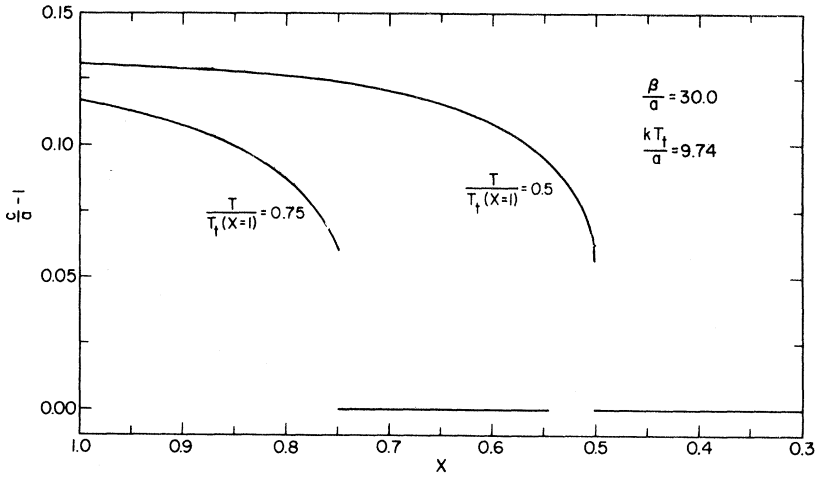

FIG. 13. Axial ratio as function of the concentration. $c/a-1$ is shown at two temperatures for the strong anisotropic-coupling system (III), whose parameters are shown in Fig. 11.

Fig. 11) and are drawn for two values of $T/T_t(x=1)$, where $T_t(x=1)$ denotes the transition temperature of the pure system III.

For a fixed value of the temperature a characteristic critical concentration x_c exists, below which the tetragonal phase becomes unstable. This critical concentration is well established experimentally.[4,45-48] It, as well as the associated axial distortion $c/a-1$, decreases with decrease of temperature, as one can see from the figure.

There is also experimental evidence[46,48] for the existence of a *minimal* critical concentration, below which the system remains cubic no matter how low the temperature may be. This behavior may be due to a clustering effect[48-50] or to the correlation between distortions. Since the present theory deals with a homogeneous crystal and does not include short-range correlation, it does not predict a minimal critical concentration.

Qualitatively, similar behavior of the axial ratio to that shown in Fig. 13 was observed in $MgAl_2O_4$ mixed with either Mn_3O_4 or $MgMn_2O_4$,[47] in $(ZnMn_2O_4)_x$ $(Cu_2Ge\ O_4)_{1-x}$[51] and in $Cu_{1-z}Zn_zCr_2O_4$.[52] On the other hand, the singular depression of c/a near x_c is missing in the mixed cobalt and manganese spinels,[42] or in $Mg_zMn_{3-z}O_4$.[41]

VI. CONCLUSION

We have shown how the cooperative manifestation of the JT effect can be treated in a molecular field type approximation scheme, retaining the dynamic character of the ionic motion. In this work the phase transition in the spinel structure has been studied; the application of the present method to the perovskite structure will be given in a later work.

The salient approximations or assumptions on which the theory of this paper is based are: First, the reliance on the molecular field approximation. We intend to improve the method by including short-range correlations. Second, we assumed the cations to be locked in their positions and the A-type ions to be absent. We discussed the import of these assumptions in the paper. Third, the extremely strong linear coupling case was treated. This amounted to forcing the radial coordinate q of the doubly degenerate vibrational mode of each octahedron to take the value $q=q_0=L/2\hbar\omega$. If this restriction is removed, one would not expect the process of the phase transition, which is primarily an orientational phenomenon, to change essentially, except insofar that the quantity q_0 [or the related parameter γ_θ, see Eq. (11)] appearing in the expression will not have the value as above. Instead q_0 will in fact depend in a complicated way on most other parameters of the problem, e.g., β (the nonlinear coupling constant), λ (the molecular field strength parameter), and most importantly, on the temperature T. It is not evident, without the development of a specific model for the interionic interactions, which way the value of q_0 will vary with T, and we do not expect this variation to be much larger than that due to anharmonicity, which was neglected here. Without question, the change of, for example, the axial ratio with temperature (see Fig. 12) near T_t will be dominated by cooperative orientational effects and not by the temperature variation of q_0.

Fourth, we have used localized vibrational modes instead of phonons. It seems that, in the present case where the cooperative phenomenon is due to displacements, the proper use of the latter is tantamount to a rigorous solution of the problem, whereas the employment of the former fits in well with the molecular field approximation. True, Kanamori[6] studied the cooperative problem through the $\vec{k}=0$ phonon. However, the other phonons ($\vec{k}\neq 0$) were not included, so that the fluctuat-

ing aspects of the phenomena were absent.

We have neglected spin-orbit coupling on the cations. This would split the Mn^{3+} ground-state term into five states (spaced less than 10 cm^{-1} apart) and for Cu^{2+} would invoke a coupling of the Γ_8 state with triply degenerate vibrations. Both effects are much weaker (except very near T_t) than the tetragonal molecular field, which being between twice and four times kT_t (Fig. 9), is characteristically several 100 cm^{-1}. For low concentrations of the JT ions the situation may alter, however.

Concluding, there is a great need for more experiments, especially thermal data, to confirm the theory here outlined. It is strongly felt that the property of the homogeneous crystal must be clearly understood, before further effects, e.g., clustering, important in themselves or for applications, can be treated.

ACKNOWLEDGMENTS

We thank Professor M. Luban and B. Barnett for discussions, and Dr. F. S. Ham for correspondence. The numerical data were obtained on the CDC 3400 computer of Tel-Aviv University while the first-named author was a visiting part-time associate professor.

APPENDIX: STRONG MOLECULAR FIELD LIMIT

The matrix elements of the Hamiltonian on the left-hand side of Eq. (10), but without the constant term E_q, are denoted in the representations $\cos\frac{1}{2}\times(2m-1)\varphi$ and $\sin\frac{1}{2}(2m-1)\varphi$ for $m=1,2,\ldots$ by C_{mn} and S_{mn}, respectively, where the nonvanishing matrix elements are in the cosine representation:

$$C_{mm}=\tfrac{1}{4}\alpha(2m-1)^2+\gamma_\theta^2/2\lambda\hbar\omega q_0^2, \quad (m\neq 1,2)$$
$$C_{11}=\tfrac{1}{4}\alpha-\tfrac{1}{2}\gamma_\theta+\gamma_\theta^2/2\lambda\hbar\omega q_0^2,$$
$$C_{22}=\tfrac{9}{4}\alpha-\tfrac{1}{2}\beta+\gamma_\theta^2/2\lambda\hbar\omega q_0^2,$$
$$C_{mn}=-\tfrac{1}{2}\beta, \qquad m=n\pm 3$$
$$=-\tfrac{1}{2}\gamma_\theta, \qquad m=n\pm 1,$$
$$C_{13}=C_{31}=-\tfrac{1}{2}\beta,$$

and in sine representation:

$$S_{mm}=\tfrac{1}{4}\alpha(2m-1)^2+\gamma_\theta^2/2\lambda\hbar\omega q_0^2, \quad (m\neq 1,2)$$
$$S_{11}=\tfrac{1}{4}\alpha+\tfrac{1}{2}\gamma_\theta+\gamma_\theta^2/2\lambda\hbar\omega q_0^2,$$
$$S_{22}=\tfrac{9}{4}\alpha+\tfrac{1}{2}\beta+\gamma_\theta^2/2\lambda\hbar\omega q_0^2,$$
$$S_{mn}=-\tfrac{1}{2}\beta, \quad m=n\pm 3$$
$$=-\tfrac{1}{2}\gamma_\theta, \quad m=n\pm 1,$$
$$S_{13}=S_{31}=+\tfrac{1}{2}\beta.$$

The Hamiltonian matrix is the direct sum of the two matrices. For large molecular fields, region d in Sec. V, $\gamma_\theta\gg\alpha$ and $\gamma_\theta\gg\beta$, one finds matrices of the form

$$-\tfrac{1}{2}\gamma_\theta\begin{bmatrix} \pm 1 & 1 & 0 & 0 & \cdot & \cdot \\ 1 & 0 & 1 & 0 & \cdot & \cdot \\ 0 & 1 & 0 & 1 & \cdot & \cdot \\ 0 & 0 & 1 & 0 & \cdot & \cdot \\ \cdot & \cdot & \cdot & \cdot & \cdot & \cdot \end{bmatrix}+\frac{\gamma_\theta^2}{2\lambda\hbar\omega q_0^2},$$

where the sign in the (1, 1) position is positive (negative) in the cosine (sine) representation. Consider for a moment the above matrix to be of size $N\times N$. If N is large, the effect of the (1, 1) term is negligible (cf. the eigenfrequencies of a large, finite, harmonic linear chain) and the eigenvalues become

$$E_n=-\gamma_\theta\cos(2\pi n/N)+\gamma_\theta^2/2\lambda\hbar\omega q_0^2 \quad (n=1,2,\ldots N).$$

The partition function is

$$e^{-F/kT}=2\exp[-\gamma_\theta^2/2\lambda\hbar\omega q_0^2 kT]\times\textstyle\sum_n\exp[\gamma_\theta\cos(2\pi n/N)/kT]$$
$$\simeq(N/\pi)\exp(-\gamma_\theta^2/2\lambda\hbar\omega q_0^2 kT)\times\int_0^{2\pi}\exp(-\gamma_\theta\cos\alpha/kT)d\varphi$$
$$=2N\exp(-\gamma_\theta^2/2\lambda\hbar\omega q_0^2 kT)I_0(\gamma_\theta/kT),$$

where I_0 is the modified Bessel function of order zero.[53] The self-consistency equation, $\partial F/\partial\gamma_\theta=0$, Eq. (9) or (14), can be written

$$\frac{kT}{\lambda\hbar\omega q_0^2}=\frac{I_1(\gamma_\theta/kT)}{(\gamma_\theta/kT)I_0(\gamma_\theta/kT)}. \tag{A1}$$

On the other hand, the equation [Eq. (15)], $F(\gamma_\theta)=F(0)$ which holds at the transition temperature T_t yields

$$I_0(\gamma_{\theta,t}/kT_t)=\exp(\gamma_{\theta,t}^2/2\lambda\hbar\omega q_0^2 kT_t),$$

where $\gamma_{\theta,t}$ is the value of γ_θ at $T=T_t$. The last equation has real solutions only when the arguments of both the Bessel function and the exponential vanish. Taking the limit of the right-hand side of (A1) for $\gamma_{\theta,t}/kT_t\to 0$, we obtain for the left-hand side $kT_t/\lambda\hbar\omega q_0^2=\frac{1}{2}$. This is the asymptotic value, for $\lambda\hbar\omega q_0^2/(\alpha\beta)^{1/2}\to\infty$, which appears on the right-hand edge of Fig. 9.

[1]J. D. Dunitz and L. E. Orgel, J. Phys. Chem. Solids 3, 20 (1957).

[2]D. S. McClure, J. Phys. Chem. Solids 3, 311 (1957).

[3]J. B. Goodenough, *Magnetism and the Chemical Bond* (Interscience, New York, 1963).

[4]G. I. Finch, A. P. B. Sinha, and K. P. Sinha, Proc. Roy. Soc. (London) A242, 28 (1957).

[5]P. J. Wojtowicz, Phys. Rev. 116, 32 (1959).

[6]J. Kanamori, J. Appl. Phys. Suppl. 31, 14 (1960); J. Kanamori, M. Kataoka, and Y. Itoh, *ibid.* 39, 688 (1968).

[7]R. Brout, *Phase Transitions* (Benjamin, New York, 1965), Sec. 2-2.

[8]S. J. Allen, Phys. Rev. 166, 530 (1968); 167, 492 (1968).

[9]M. Tanaka, T. Tokoro, and Y. Aiyama, J. Phys. Soc. Japan 21, 262 (1966).

[10]F. Hartmann-Boutron and P. Imbert, J. Appl. Phys. 39, 775 (1968).

[11]J. B. Goodenough and A. L. Loeb, Phys. Rev. 98, 391 (1955).

[12]U. Ganiel and S. Shtrikman, Phys. Rev. 167, 258 (1968).

[13]U. Öpik and M. H. L. Pryce, Proc. Roy. Soc. (London) A238, 425 (1957).

[14]Other types of further neighbor interactions that we tried, e.g., along each face diagonal, lead to the same result, Eq. (2) below.

[15]W. Moffitt and A. D. Liehr, Phys. Rev. 106, 1195 (1957).

[16]H. C. Longuet-Higgins, U. Öpik, M. H. L. Pryce, and R. A. Sack, Proc. Roy. Soc. (London) A244, 1 (1958).

[17]M. S. Child and H. C. Longuet-Higgins, Phil. Trans. Roy. Soc. 254, 259 (1961).

[18]M. C. M. O'Brien, Proc. Roy. Soc. (London) A281, 323 (1964).

[19]I. B. Bersuker, Zh. Eksperim. i Teor. Fiz. 43, 1315 (1962); 44, 1239 (1963) [Soviet. Phys. JETP 16, 933 (1963); 17, 836 (1963)].

[20]J. Slonczewski, Phys. Rev. 131, 1596 (1963).

[21]K. A. Müller, IBM Research Paper No. RZ-222, 1967 (unpublished).

[22]M. H. L. Pryce, K. P. Sinha, and Y. Tanabe, Mol. Phys. 9, 33 (1965).

[23]L. L. Lohr, Jr., Inorg. Chem. 6, 1890 (1967).

[24]M. D. Sturge, in *Solid State Physics*, edited by F. Seitz, D. Turnbull, and H. Ehrenreich (Academic, New York, 1967), Vol. 20, p. 91.

[25]F. S. Ham, in *Electron Paramagnetic Resonance*, edited by S. Geschwind (Plenum, New York, 1969).

[26]R. Englman, *The Jahn-Teller Effect* [Wiley-Interscience, New York, (to be published)].

[27]J. S. Griffith, *The Irreducible Tensor Method for Molecular Symmetry Groups* (Prentice-Hall, Englewood Cliffs, N. J., 1962).

[28]B. Halperin and R. Englman (unpublished).

[29]B. Halperin and R. Englman, Solid State Commun. 7, 1579 (1969).

[30]F. I. B. Williams, D. C. Krupka, and D. P. Breen, Phys. Rev. 179, 255 (1969).

[31]U. T. Höchli, Phys. Rev. 162, 262 (1967).

[32]U. T. Höchli and T. L. Estle, Phys. Rev. Letters 18, 128 (1967).

[33]R. E. Coffman, Phys. Letters 19, 475 (1965); 21, 381 (1966); J. Chem. Phys. 48, 609 (1968).

[34]M. S. Child, Mol. Phys. 5, 391 (1962); M. S. Child and H. L. Strauss, J. Chem. Phys. 42, 2282 (1965).

[35]J. C. Slouczewski, Solid State Commun. 7, 519 (1969).

[36]L. D. Landau and E. M. Lifshitz, *Statistical Physics* (Pergamon, Oxford, England, 1959), Chap. 14.

[37]C. Haas, J. Phys. Chem. Solids 26, 1225 (1965).

[38]J. F. Nye, *Physical Properties of Crystals* (Pergamon, Oxford, England, 1957), p. 134.

[39]A. B. Pippard, *Elements of Classical Thermodynamics* (Cambridge U. P., Cambridge, England, 1957), p. 61.

[40]K. S. Irani, A. P. B. Sinha, and A. B. Biswas, J. Phys. Chem. Solids 23, 711 (1962).

[41]M. Rosenberg, P. Nicolau, R. Manaila, and P. Pausescu, J. Phys. Chem. Solids 24, 1419 (1963).

[42]I. Aoki, J. Phys. Soc. Japan 17, 53 (1962).

[43]T. Inoue and S. Iida, J. Phys. Soc. Japan 13, 656 (1958).

[44]H. Ohnishi, T. Teranishi, and S. Miyahara, J. Phys. Soc. Japan 14, 106 (1959).

[45]H. F. McMurdie, B. M. Sullivan, and F. A. Mauer, J. Res. Natl. Bur. Std. 45, 35 (1950).

[46]D. G. Wickham and W. J. Croft, J. Phys. Chem. Solids 7, 351 (1958).

[47]K. S. Irani, A. P. B. Sinha, and A. B. Biswas, J. Phys. Chem. Solids 17, 101 (1960).

[48]L. Cervinka and D. Vetterkind, J. Phys. Chem. Solids 29, 171 (1968).

[49]D. B. Rogers, R. W. Germann, and R. J. Arnott, J. Appl. Phys. 36, 2338 (1965).

[50]J. B. Goodenough, J. Appl. Phys. 36, 2342 (1965).

[51]M. Robbins and P. K. Baltzer, J. Appl. Phys. 36, 1039 (1965).

[52]Y. Kino and S. Miyahara, J. Phys. Soc. Japan 21, 2732 (1966).

[53]I. S. Gradshteyn and I. M. Ryzhik, *Tables of Integrals, Series, and Products* (Academic, New York, 1965), p. 958.